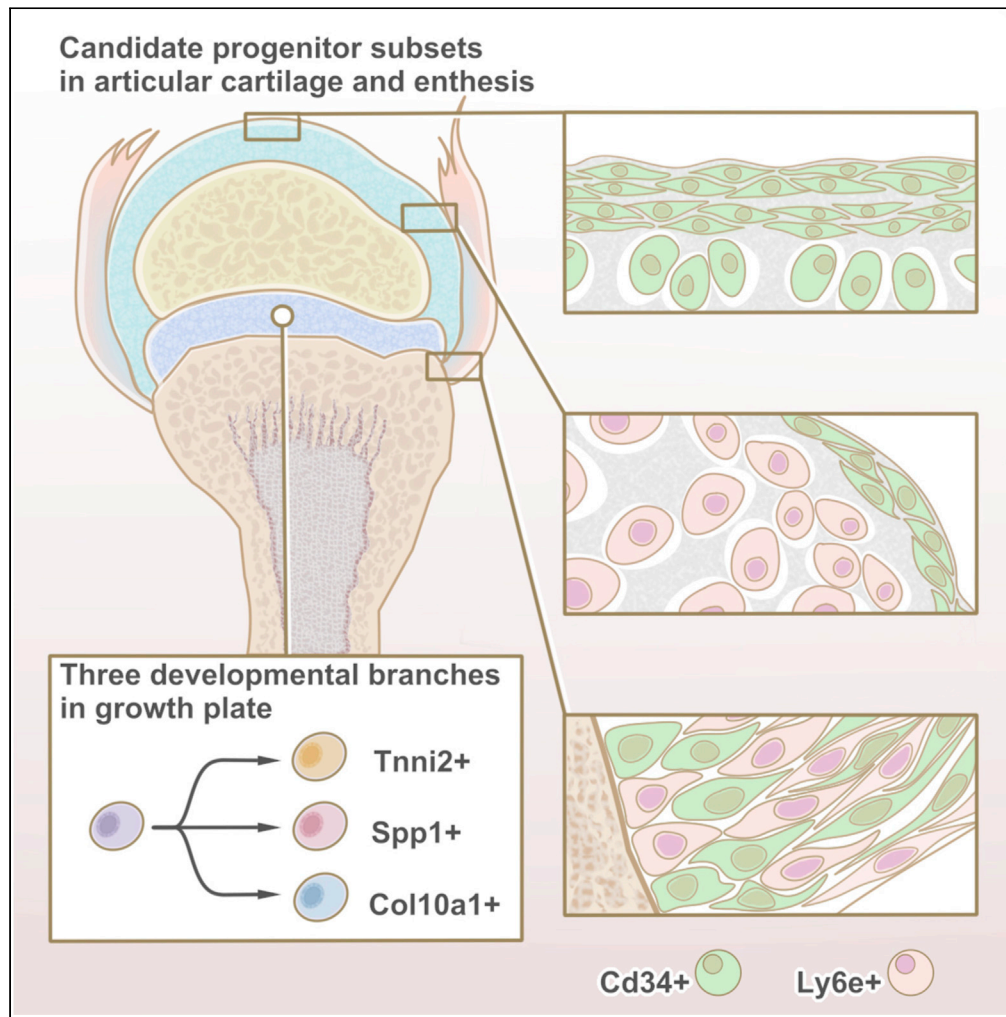


Article

# Deciphering postnatal limb development at single-cell resolution



Manman Gao, Xizhe Liu, Peng Guo, ..., Dafu Chen, Xuenong Zou, Zhiyu Zhou

szhzw@mail.szu.edu.cn (W.Z.)  
 chendafujst@126.com (D.C.)  
 zouxuen@mail.sysu.edu.cn (X.Z.)  
 zhouzhy23@mail.sysu.edu.cn (Z.Z.)

**Highlights**

Delineation of postnatal limb developmental landscape

Discovery of candidate progenitors in articular cartilage and entheses

Parsing of three cellular developmental branches in postnatal growth plate

Reaching interconnections of postnatal limb development and pathological remodeling

Gao et al., iScience 26, 105808  
 January 20, 2023 © 2022 The Author(s).  
<https://doi.org/10.1016/j.isci.2022.105808>

## Article

## Deciphering postnatal limb development at single-cell resolution

Manman Gao,<sup>1,2,5,6</sup> Xizhe Liu,<sup>5</sup> Peng Guo,<sup>1,5</sup> Jianmin Wang,<sup>1,5</sup> Junhong Li,<sup>1,5</sup> Wentao Wang,<sup>1,5</sup> Martin J. Stoddart,<sup>3</sup> Sibylle Grad,<sup>3</sup> Zhen Li,<sup>3</sup> Huachuan Wu,<sup>1,5</sup> Baoliang Li,<sup>1,5</sup> Zhongyuan He,<sup>1,5</sup> Guangqian Zhou,<sup>6</sup> Shaoyu Liu,<sup>1,5</sup> Weimin Zhu,<sup>2,6,\*</sup> Dafu Chen,<sup>4,\*</sup> Xuenong Zou,<sup>5,\*</sup> and Zhiyu Zhou<sup>1,5,7,\*</sup>

## SUMMARY

**The early postnatal limb developmental progression bridges embryonic and mature stages and mirrors the pathological remodeling of articular cartilage. However, compared with multitudinous research on embryonic limb development, the early postnatal stage seems relatively unnoticed. Here, a systematic work to portray the postnatal limb developmental landscape was carried out by characterization of 19,952 single cells from murine hindlimbs at 4 postnatal stages using single-cell RNA sequencing technique. By delineation of cell heterogeneity, the candidate progenitor sub-clusters marked by *Cd34* and *Ly6e* were discovered in articular cartilage and enthesis, and three cellular developmental branches marked by *Col10a1*, *Spp1*, and *Tnni2* were reflected in growth plate. The representative transcriptomes and developmental patterns were intensively explored, and the key regulation mechanisms as well as evolvement in osteoarthritis were discussed. Above all, these results expand horizons of postnatal limb developmental biology and reach the interconnections between limb development, remodeling, and regeneration.**

## INTRODUCTION

Limb development is a highly orchestrated process. In the past decades, limb ontogeny,<sup>1</sup> patterning,<sup>2</sup> and morphogenesis<sup>3</sup> during embryonic stage have been intensively studied.<sup>4</sup> Nowadays, increasing attention has been focused on the interconnections between limb development, remodeling, and regeneration.<sup>5,6</sup> Compared with embryonic developmental process, postnatal limb development, a process involving diversified cell lineages cross-talked with the relatively mature extra-cellular matrix micro-environment to coordinate recruitment, proliferation, and differentiation, is a magnificent spectacle connected with embryonic rudiment formation and mapped into tissue remodeling and regeneration.

During postnatal stage, the limb is one orchestrated composite of diverse cellular types. In murine long bones, the secondary ossification center (SOC) develops postnatally, when the articular cartilage and subchondral bone develop, mature, and separate from one entire cartilage template.<sup>7</sup> With SOC formation, the heterogeneity of epiphyseal growth plate (GP) chondrocytes reaches its peak, when exactly the epiphyseal stem cells generate.<sup>7-9</sup> Hitherto, the cellular biological heterogeneity of GP chondrocytes lacks deeper parsing. For articular cartilage, zonal organization and maturation also occur postnatally. Although previous studies have identified the presence of cells with a progenitor or stem character in the superficial zone of adult articular cartilage,<sup>10-12</sup> the variation of self-regenerative capability encouraged us to consider the heterogeneity of the progenitor cell reservoir with age.

In the present study, considering current limitation in the understanding of postnatal limb developmental biology, we systematically mapped the cell atlas of murine postnatal limbs by single-cell RNA sequencing (scRNA-seq). By dissecting the cellular heterogeneity, we identified clusters marked by *Cd34* and *Ly6e* in articular cartilage and evolutionary branches marked by *Col10a1*, *Spp1*, and *Tnni2* in GP. The evolvement in both development and osteoarthritis was discussed, reaching further understanding of the interconnections between limb development, remodeling, and regeneration.

<sup>1</sup>Department of Orthopaedic Surgery, The Seventh Affiliated Hospital, Sun Yat-sen University, Shenzhen 518107, China

<sup>2</sup>Department of Sport Medicine, Institute of Translational Medicine, The First Affiliated Hospital of Shenzhen University, Shenzhen Second People's Hospital, Shenzhen 518035, China

<sup>3</sup>AO Research Institute Davos, Davos 7270, Switzerland

<sup>4</sup>Laboratory of Bone Tissue Engineering, Beijing Laboratory of Biomedical Materials, Beijing Research Institute of Orthopaedics and Traumatology, Beijing JiShuiTan Hospital, Beijing 100035, China

<sup>5</sup>Guangdong Provincial Key Laboratory of Orthopedics and Traumatology, The First Affiliated Hospital of Sun Yat-sen University, Guangzhou 510080, China

<sup>6</sup>Shenzhen Key Laboratory of Anti-aging and Regenerative Medicine, Department of Medical Cell Biology and Genetics, Health Sciences Center, Shenzhen University, Shenzhen 518071, China

<sup>7</sup>Lead contact

\*Correspondence: szhzw@mail.szu.edu.cn (W.Z.), chendafujst@126.com (D.C.), zouxuen@mail.sysu.edu.cn (X.Z.), zhouchy23@mail.sysu.edu.cn (Z.Z.)

<https://doi.org/10.1016/j.isci.2022.105808>



## RESULTS

### Cell diversity of murine hindlimb delineated by single-cell transcriptomic analysis

To systematically parse the postnatal limb developmental process, murine hindlimbs of postnatal day 1 (P1), day 5 (P5), day 14 (P14), and day 28 (P28) were used for scRNA-seq (Figures 1A and S1A). Here, we profile the transcriptomes of 19,952 single cells with an average of 3,282 genes detected in each individual cell after quality control. At each time point, 3,048, 5,803, 6,325, and 4,776 cells were delineated, respectively. All single-cell transcriptomes were subjected to Louvain clustering and uniform manifold approximation and projection (UMAP) visualization, revealing 23 subsets unequally distributed at each time point (Figures S1B and S1C). According to feature genes expression, the cellular type of each subset was recognized and annotated (Figures 1A, 1B, and S1D), including GP chondrocytes (*Epyc*, *Matn1*, *Matn3*, and *3110079O15Rik/Snorc*),<sup>13,14</sup> articular chondrocytes (*Prg4*, *Cytl1*, *Wif1*, *Acvr1*, and *Dlk1*),<sup>15,16</sup> entheses cells (*Aspn*, *Fstl1*, *Postn*, *Ptn*, *Lgals1*, *Vcan*, and *Mmp13*),<sup>17,18</sup> endothelial cells (ECs, *Kdr*, *Pecam1/Cd31*, and *Emcn*),<sup>19,20</sup> mural cells (MCs, *Des*, *Mcam*, *Tagln*, and *Notch3*),<sup>21</sup> hematopoietic cells (*Ptpcr* and *Spi1*),<sup>22,23</sup> and erythron (*Gypa*).<sup>24</sup> Subsets belonging to one cellular type had closer links shown by partition-based graph abstraction (PAGA) analysis<sup>25</sup> (Figure S1E). MCs included with the vascular smooth muscle cells (SMCs, *Myh11*, *Acta2*, and *Tagln*)<sup>26</sup> and pericytes (*Pdgfrb*, *Rgs5*, *Des*, *Abcc9*, and *Kcnj8*)<sup>27</sup> (Figures 1C and 1D). In the hematopoietic cells, several hematopoietic lineage commitment progenitors (HLCs) were recognized, including dendritic cell lineage (*Siglech*, *Ly6d*, *Ccr9*, *Sla2*, *Cox6a2*, and *Tlr7*),<sup>28</sup> mast cell lineage (*Fcgr3*, *Cpa3*, *Gata2*, *Cd200r3*, and *Mcpt8*),<sup>29</sup> T cell lineage (*Txk*, *Cd3d*, *Il2rb*, *Trbc1*, *Trbc2*, and *Cd28*),<sup>30</sup> monocyte lineage (*Ccr2*, *Ly6c2*, *Ms4a6c*, *Ctsc*, *Cfp*, and *Htr7*),<sup>31</sup> neutrophil lineage (*Mpo*, *Elane*, *Ms4a3*, *Prtn3*, *Cst7*, and *Ctsg*),<sup>32,33</sup> and erythroid lineage (*Gata1*, *Mfsd2b*, *Ache*, *Gfi1b*, *Samd14*, and *Epor*)<sup>34</sup> (Figures S1F–S1H). Accordingly, mononuclear phagocyte system (MPS; *Cd68*, *Msr1*, *Csf1r*, and *Acp5*),<sup>35</sup> neutrophils (*Wfdc21*, *S100a8/9*, and *Ly6g*)<sup>36</sup> and B cell lineage (*Cd79a/b*, *Ebf1*, *Blk*, and *Cd19*)<sup>37</sup> were also identified. In the MPS subset, pre-osteoclasts (pre-OC, *Csf1r*, *Adgre1*, *C1qa*, *C1qb*, *C1qc*, *Aif1*, *Trem2*, and *C3ar1*)<sup>38–40</sup> and osteoclasts (OC, *Acp5*, *Tnfrsf11a*, *Nfatc1*, *Mmp9*, and *Ctsk*)<sup>41</sup> were identified (Figures 1F–1G). The above subsets exhibited unevenly developed distribution at different ages (Figures 1E, 1H, S1I, and S1J). Briefly, most hematopoietic cell lineages concentrated at P28 when the SOC preliminarily matured; however, the osteoclast lineage generated at P01 and peaked at P14 (Figure 1H), and the ECs and MCs were expanded as early as P01 (Figure 1E), coincided with previous studies on epiphyseal cartilage remodeling mediated by osteochondroclasts<sup>42</sup> and vascularization.<sup>43</sup>

### Integrated analysis of the GP, articular cartilage, and entheses

GP, articular cartilage, and entheses were characterized as the main limb connective tissues, which were extracted for further analysis. First, dimensionality reduction was performed and 18 subsets were delineated by UMAP visualization (Figure S2A). According to feature genes expression, small subsets of glial cells (*Plp1*, *Mpz*, *Sox2*, and *Egfl8*) and muscle cells (*Myod1*, *Msc*, and *Des*) were recognized<sup>44</sup> (Figures 2A and S2B). PAGA analysis showed more strong corrections among subsets belonging to the same tissue type (Figure S2C). The GP chondrocytes, AC, and entheses cells were ordered along a pseudotime trajectory.<sup>45</sup> Overlapped distribution of AC with both GP chondrocytes and entheses cells suggested their interconnections during limb development<sup>46</sup> (Figure 2B), which was consistent with the pseudotemporal ordering of the feature genes (Figure S2D).

As widely concerned, the expression pattern of key transcription factors (TFs) and signaling factors was analyzed. Five distinct gene expression patterns were identified after ordering all differentially expressed TFs along the trajectory axis (Figures 2C and S2E). TFs in pattern 1 were highly expressed in both GP and AC, which were required for chondrocyte lineage commitment, such as *Sox9*<sup>47</sup> or chondrocyte terminal differentiation, including *Foxa3* and *Foxc1*.<sup>48,49</sup> TFs in pattern 2 were mostly restricted in GP and functioned as regulators of cartilage development including *Barx2*<sup>50</sup> and *Runx3*.<sup>51</sup> *Hmga* genes were all ordered by pattern 3, which were highly expressed in AC and functioned in maintaining AC homeostasis.<sup>52</sup> In pattern 4, TFs showed up-regulated in both AC and EN, including *Cebpz*, *Mef2a*, *Tcf4i*, and *Zfp361/2*, etc., which functioned in muscle and tendon development<sup>53–55</sup> and osteoarthritis progression.<sup>56,57</sup> Genes in pattern 5 were primarily expressed in EN, which were proved involved in connective tissue development. It is to be highlighted that several TFs in pattern 2 (*Mef2c*, *Runx2*, and *Shox2*, etc.) and pattern 5 (*Ebf1* and *Maf*, etc.) were enriched in both GP and EN and are recognized as regulators of chondrocyte hypertrophy, osteogenesis, and mineralization. For key signaling factors, 6 gene expression patterns were revealed (Figures 2D and S2F). In detail, *Bmp* signaling showed most intense expression in AC, with *Bmp2*, *Bmp5*, *Bmp6*, and *Acvr1* being highly expressed. *Tgfb* factors showed increased expression in AC and EN, with low

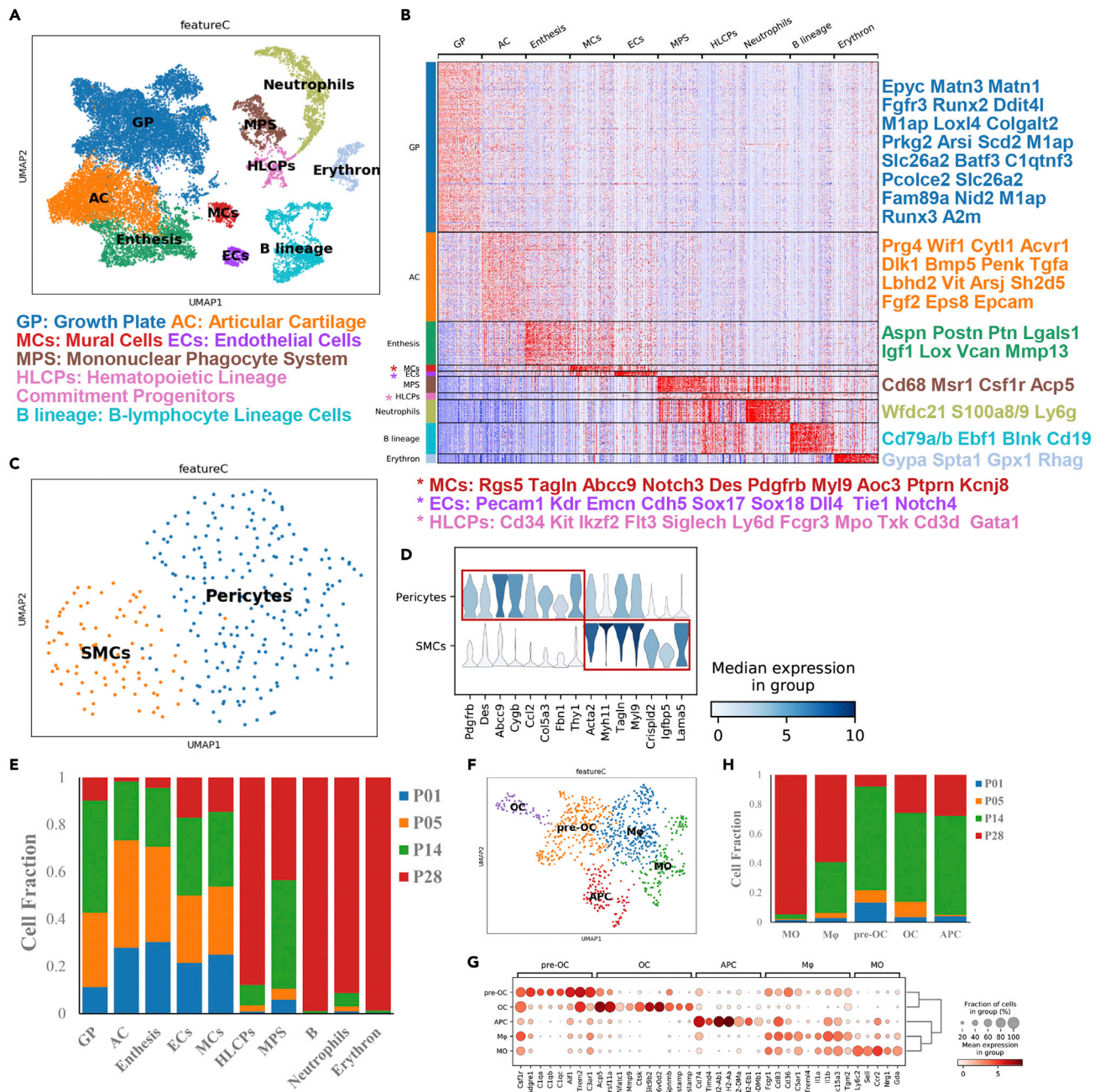


**Figure 1. Overall parsing of murine postnatal hindlimbs**

(A) UMAP visualization of all interpreted cell types from murine hind limbs at 4 postnatal stages.

(B) Heatmap denoting genes enriched in each type of cell subset.

(C) UMAP visualization of MCs, indicating two cell types including SMCs and pericytes.

(D) Violin plots showing feature genes of pericytes and SMCs.

(E) Fraction of cells from different postnatal stages in each type of cell subset in (A).

(F) UMAP visualization of MPS, revealing five cell types including monocytes (MO), macrophages (Mφ), antigen-presenting cells (APC), pre-OC, and OC.

(G) Fraction of cells from different postnatal stages in each subset of MPS.

(H) Dot plots showing the expression of curated feature genes in each subset of MPS.

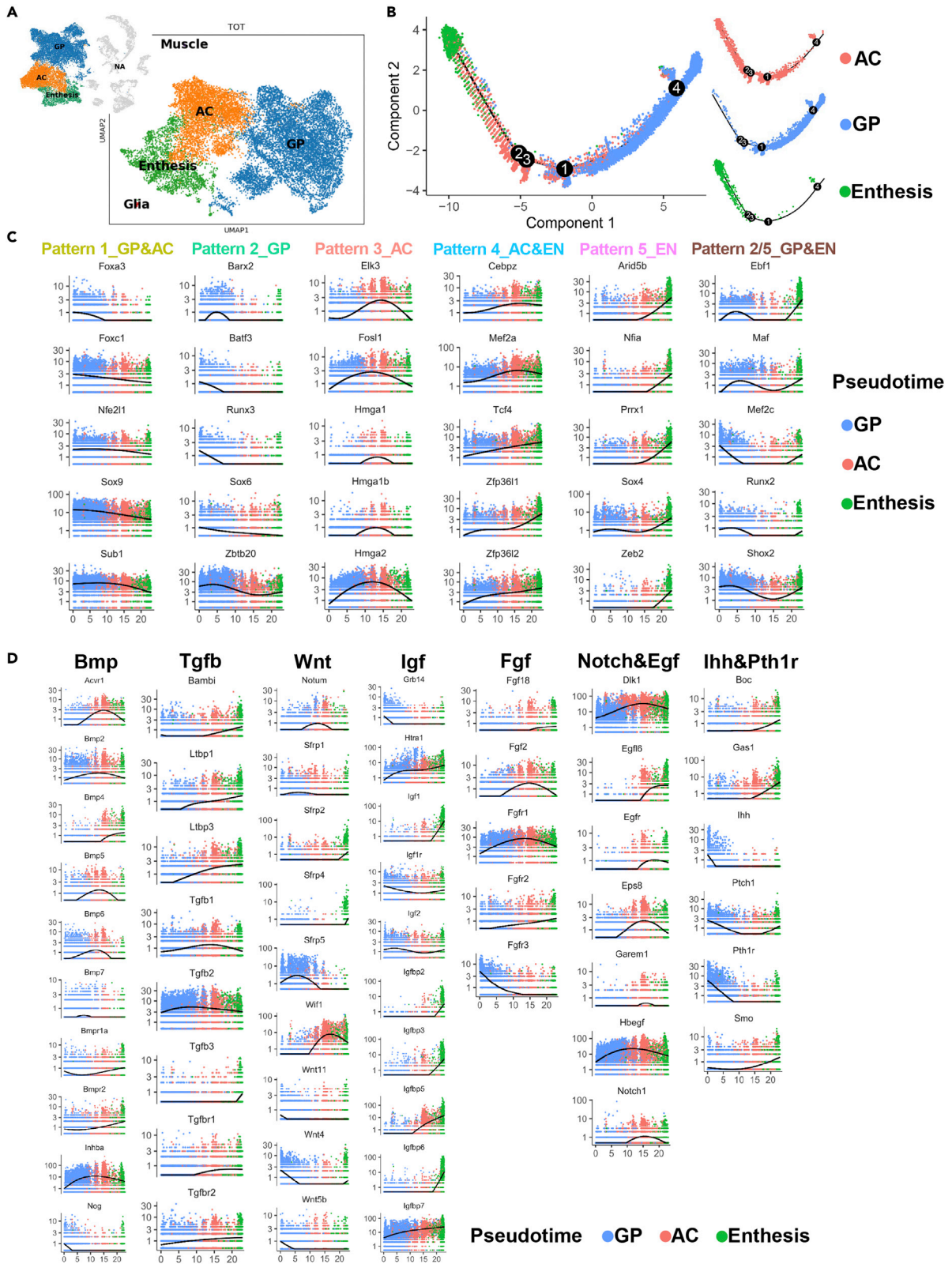


**Figure 2. Integrated analysis of the GP, articular cartilage, and enthesis**

- (A) Identities of cells from GP, articular cartilage (AC), and enthesis in Figure 1A by UMAP visualization revealing five cell types including GP, AC, enthesis, muscle cells, and glial cells.
- (B) Pseudotime trajectory of GP, AC, and enthesis in (A) (Left), and the distribution of cells from individual cluster (Right).
- (C) Expression of representative TFs of each pattern along pseudotime axis inferred by Monocle 2.0.
- (D) Expression of representative signaling factors of each pattern along pseudotime axis inferred by Monocle 2.0.

expression level in GP. However, *Wnt* ligands including *Wnt4*, *Wnt5*, and *Wnt11* were enriched in GP, while *Wnt* inhibitors were highly expressed in AC and EN, including *Notum* and *Wif1*. *Igf* factors were primarily expressed in EN, except for *Igf2* and *Grb14*, which were enriched in GP. *Fgf* pathways exhibited disparate patterns in AC (*Fgf2* and *Fgfr1*), GP (*Fgfr3*), or EN (*Fgf18* and *Fgfr2*). *Egf* and *Notch* signaling factors were enriched in AC, and *Ihh* and *Pth1r* signaling functioned mainly in GP and EN.

The aforementioned regulators weaved an intricate and precise network directing the specific tissue development. Nonetheless, elaboration of the common regulating patterns would be conducive to understanding the relevant biological process in both development and disease, including chondrocyte hypertrophy and extracellular matrix mineralization. Next, we analyzed each cell subset focusing on interpretation of the developmental and cell biology, with discussion of the correlation between development and degeneration.

**Interpretation of *Cd34*<sup>+</sup> cell cluster and *Ly6e*<sup>+</sup> cell cluster in developmental articular cartilage**

As an intermediate tissue interconnecting GP and enthesis during development, AC were interpreted into 4 clusters (Figures 3A and S3A). Cluster 4 expressed both AC and EN feature genes (AC\_EN), cluster 5 expressed both AC and GP feature genes (AC\_GP), cluster 14 was in cell cycle (AC\_ *Mki67*<sup>+</sup>), and cluster 0 only highly expressed characteristic AC genes (AC\_AC) (Figures S3A and S3B). Consistent with the characteristic gene expression pattern, when ordered along the pseudotime trajectory of cells from AC, EN, and GP, cells of AC\_EN were mapped interconnected with AC and EN, cells of AC\_GP were distributed to intermediate AC and GP, cells of AC\_AC were restricted to AC, and the proliferating cells in cluster AC\_ *Mki67*<sup>+</sup> showed scattered distribution overlapped with each of the 3 other clusters (Figure S3C). As articular cartilage matures, the fraction of AC\_AC and proliferating chondrocytes was gradually declined, while the cell fraction of AC\_EN was increased (Figure 3B).

To understand the postnatal development of articular cartilage, the AC\_AC were separated for further analysis, with identification of four cell sub-clusters (Figure 3C). The developmental progression was reconstructed by applying the RNA velocity (Figure 3D) and pseudotime trajectory analysis (Figure S3D). AC2 was revealed as the upstream subset, directing to two trajectories of AC3 and AC4. Identically, Gene Ontology (GO) analysis<sup>58</sup> suggested that the biological process of AC2 was related with cartilage development and chondrocyte differentiation (Figure S3E). For feature genes expression analysis (Figure 3E), articular cartilage-specific genes, e.g., *Col8a1*,<sup>59</sup> *Vit*,<sup>60</sup> and *Abi3bp*,<sup>61</sup> were highly expressed in AC1 and AC2 sub-clusters. In addition, AC2 expressed *Gdf5* and *Nt5e*, which were respectively used to identify developmental joint progenitors<sup>62</sup> and prechondrocytes.<sup>63</sup> AC3 also expressed feature genes of GP chondrocyte, such as *Epyc* and *Matn1*, and suggested interconnection with AC\_GP cells. The AC4 sub-cluster, as one trajectory developed from AC2 (Figure S3D), showed enriched gene sets in negative regulation of cell development. However, *Cilp*, a marker of intermediate zone of articular cartilage,<sup>64</sup> was distributed mainly in AC4 subset, and characterization of this sub-cluster needed further exploration.

To further interpret properties of the AC2 and AC4 subsets, we searched the cell membrane protein encoding genes and identified *Cd34* in the AC2 sub-cluster and *Ly6e* in the AC4 sub-cluster (Figure 3E). Then *Cd34*<sup>+</sup> cells and *Ly6e*<sup>+</sup> cells were screened out from the AC\_AC cluster (Figure 3F). Thereinto, cell fraction of *Cd34*<sup>+</sup> sub-cluster was gradually decreased as cells mature (Figure 3G). The evolutionary trajectory was consistent with that applied in the four AC\_AC sub-clusters (Figure S3F), indicating the *Cd34*<sup>+</sup> sub-cluster as upstream. The TF expression heatmap following pseudotime analysis showed that TFs related with stemness maintenance and modulation (*Id2*, *Id3*, *Gata6*, *Foxd1*, *Tbx18*, *Pitx1*, *Junb*, *Jund*, *Prrx*, *Tcf4*, etc.) and chondrocyte lineage commitment (*Sox9* and *Sox5*) were clustered together with *Cd34*, and TFs functioned in stemness maintenance and modulation (*Nfia*, *Nfib*, *Fosl1*, *Stat5a*, *Etv5*, *Barx1*, *Foxp1*, *Irf2*, etc.) and chondrocyte terminal differentiation/osteogenesis (*Irx3*) were clustered with *Ly6e* (Figure 3H). Although, both sub-clusters expressed TFs related with stemness maintenance and modulation, the recognized

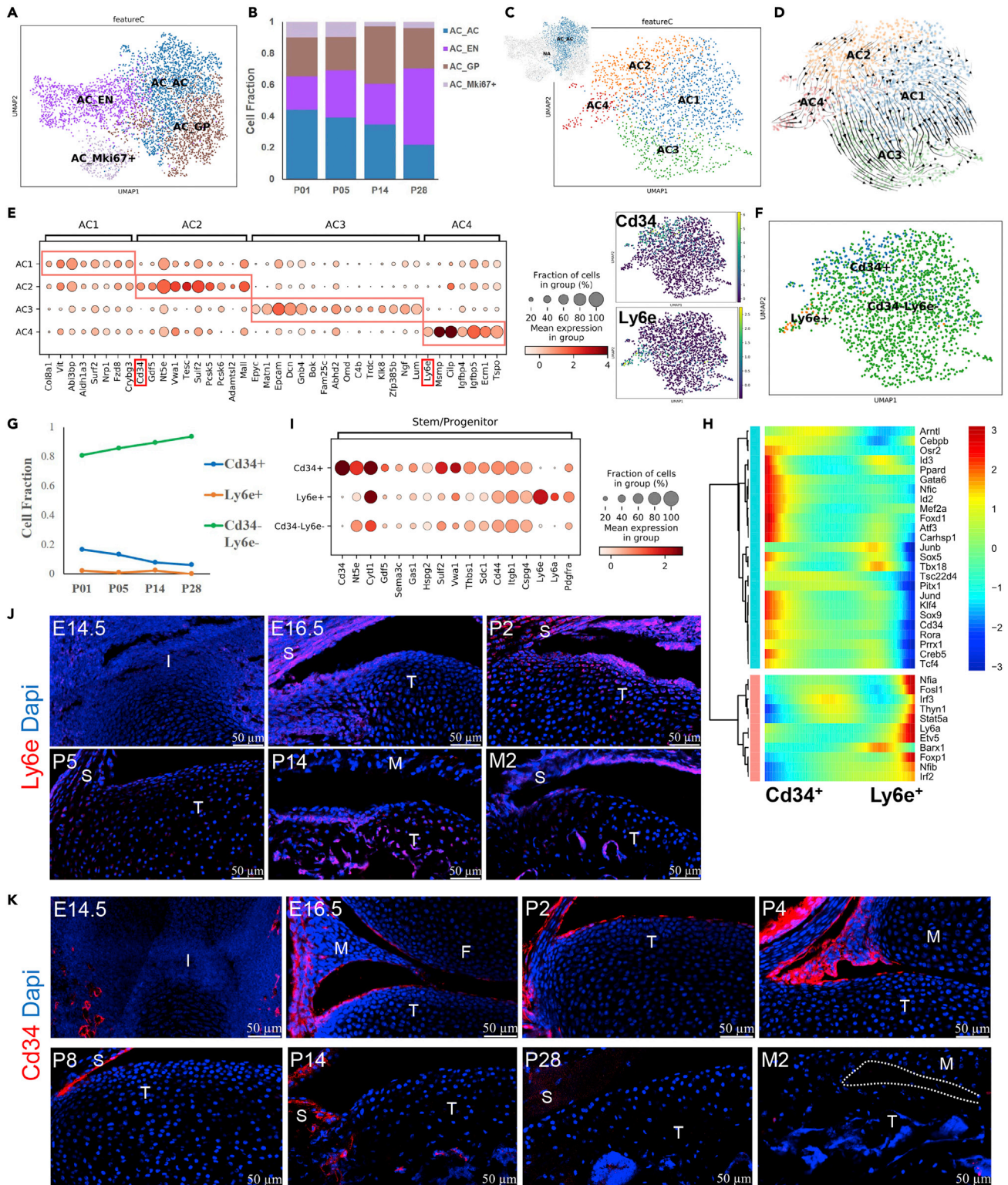


**Figure 3. Interpretation of  $Cd34^+$  cell cluster and  $Ly6e^+$  cell cluster in developmental articular cartilage**

(A) Identities of cells from AC (corresponding to Figure 2A) by UMAP visualization revealing four cell types including typical AC, chondrocytes interconnected with articular cartilage and enthesis (AC\_EN), chondrocytes interconnected with articular cartilage and growth plate (AC\_GP), and cells in cell cycle from the above three subsets (AC\_Mki67<sup>+</sup>).

**Figure 3. Continued**

- (B) Fraction of cells from different postnatal stages in each subset in (A).
- (C) Identities of cells from typical AC (corresponding to A) by UMAP visualization revealing four cell subsets referred to AC1 to AC4.
- (D) Developmental trajectory inferred by RNA velocity and visualized on the UMAP projection (corresponding to C).
- (E) Dot plots showing the expression of curated feature genes of each subset in (C) (Left) and the UMAP plots showing the expression of representative genes encoding cell membrane proteins (*Cd34* in AC2 subset and *Ly6e* in AC4 subset).
- (F) UMAP plots showing the distribution of *Cd34*<sup>+</sup> cell subset, *Ly6e*<sup>+</sup> cell subset, and *Cd34*<sup>+</sup>*Ly6e*<sup>-</sup> cell subset. Noting that there were no cells co-expressed *Cd34* and *Ly6e*.
- (G) Line chart showing the temporal variation of fraction of each subset at different postnatal stages.
- (H) Expression heatmap of curated TFs of *Cd34*<sup>+</sup> cell subset and *Ly6e*<sup>+</sup> cell subset following pseudotime analysis.
- (I) Dot plots showing the expression of feature genes denoting stem or progenitor character in *Cd34*<sup>+</sup> cell subset, *Ly6e*<sup>+</sup> cell subset, and *Cd34*<sup>+</sup>*Ly6e*<sup>-</sup> cell subset.
- (J) Immunofluorescence staining showing *Ly6e* distribution in murine hind limbs at different stages, including E14.5, E16.5, P2, P5, P14, and M2 (n = 6 at E14.5, n = 5 at E16.5, and n = 4 at other time points).
- (K) Immunofluorescence staining showing *Cd34* distribution in murine hind limbs at different stages, including E14.5, E16.5, P2, P4, P8, P14, P28, and M2 (n = 6 at E14.5, n = 5 at E16.5, and n = 4 at other time points). E: embryonic, P: postnatal. Scale bars, 50  $\mu$ m. Blue indicates DAPI staining of nuclei and red indicates *Ly6e* or *Cd34* staining. I, Interzone; S, synovium; T, tibia; M, meniscus.

cartilage stem/progenitor markers were more intensively expressed in *Cd34*<sup>+</sup> sub-cluster (Figure 3I), which was aligned with the expression pattern in AC2 sub-cluster (Figure S3G), except that *Ly6e*<sup>+</sup> cells highly expressed *Ly6a* and *Pdgfra*. Immunofluorescence staining showed that *Ly6e* localized mainly in the edge of articular cartilage and appeared with a distribution overlapped with *Ly6a* (Figures 3J and S3H). *Ly6e*<sup>+</sup> cells appeared after embryonic joint morphogenesis and gradually decreased during postnatal development but would not vanish when the articular cartilage matures (Figure 3J). *Cd34* was distributed in the surface zone and edge of articular cartilage after embryonic joint morphogenesis (P16.5) and gradually decreased to undetectable at 2 months old at which stage the articular cartilage becomes mature (Figure 3K). Together, these results suggest that *Cd34* and *Ly6e* marked different subsets of articular cartilage progenitors, which play different roles on articular cartilage development.

**Interpretation of *Cd34*<sup>+</sup> cell cluster and *Ly6e*<sup>+</sup> cell cluster in developmental entheses**

Systematically, *Cd34* was expressed mainly in AC, entheses, ECs, and HLCs, and *Ly6e* was distributed largely in ECs and hematopoietic system and marginally in GP, AC, and entheses (Figure 4A). In joint tissues, 4 subsets of *Cd34*<sup>+</sup> cells were visualized (Figure 4B), mainly derived from and characterized by entheses and articular cartilage (Figure 4C). Similarly, 3 subsets of *Ly6e*<sup>+</sup> cells were revealed in joint tissues (Figure 4D). Although more *Ly6e*<sup>+</sup> cells were derived from GP compared with *Cd34*<sup>+</sup> cells, they were mainly featured as entheses and articular cartilage (Figure 4E). The above data showed the heterogeneity of *Cd34*<sup>+</sup> sub-cluster and *Ly6e*<sup>+</sup> sub-cluster in joint tissues, suggesting their primary involvement in the development of articular cartilage and entheses. On this basis, we went on to analyze the cellular heterogeneity and lineage hierarchies within entheses with focus on *Cd34*<sup>+</sup> sub-cluster and *Ly6e*<sup>+</sup> sub-cluster.

In whole entheses, 3 subsets were recognized and annotated based on marker gene expression, including one subset that aggregated with stem/progenitor cells (EN\_SP, *Tppp3*, *Pdgfra*, *Thbs4*, *Cxcl12*, *Cd55*, and *Cd248*), one subset with moderate stem/progenitor marker gene expression (*Tppp3*, *Pdgfra*, *Thbs4*, and *Cxcl12*) but without terminal differentiation or mineralization (EN\_unM, *Csf1*, *Il1r1*, *Lhfp12*, *Hmga1/2*, and *Itga5/6*), and the last one showing terminal differentiation and mineralization (EN\_M, *Runx2*, *Alpl*, *Spp1*, and *Tnfsf11*) (Figure 4F). Specifically, *Cd34* and *Ly6e* were mainly expressed in subsets of EN\_SP and EN\_unM (Figure 4G). When plotting along the pseudotime trajectory, cells in EN\_SP and EN\_unM were separately plotted at upstream of two trajectories, which jointly terminated at EN\_M stage. *Cd34* and *Ly6e* were distributed at upstream of both trajectories, similar to the stem/progenitor marker genes like *Tppp3* and *Cd55* (Figures 4H and 4I), suggesting *Cd34*<sup>+</sup> sub-cluster and *Ly6e*<sup>+</sup> sub-cluster as heterogeneous stem/progenitor cell populations in entheses.

To investigate *Cd34*<sup>+</sup> and *Ly6e*<sup>+</sup> cell subsets in entheses, we screened out each subpopulation containing cells with double positive, single-positive or double-negative expression of *Cd34* and *Ly6e*. Consistent with the pseudotime trajectory mapping, almost all of the *Cd34*<sup>+</sup>*Ly6e*<sup>+</sup> and *Cd34*<sup>+</sup> cells and about 80% of the *Ly6e*<sup>+</sup> cells were distributed in subsets of EN\_SP and EN\_unM (Figure 4J), which were plotted upstream of both trajectories (Figure 4K). To investigate the dominant features of each subpopulation, the differentially expressed TFs were screened out and clustered in a heatmap following pseudotime analysis, showing

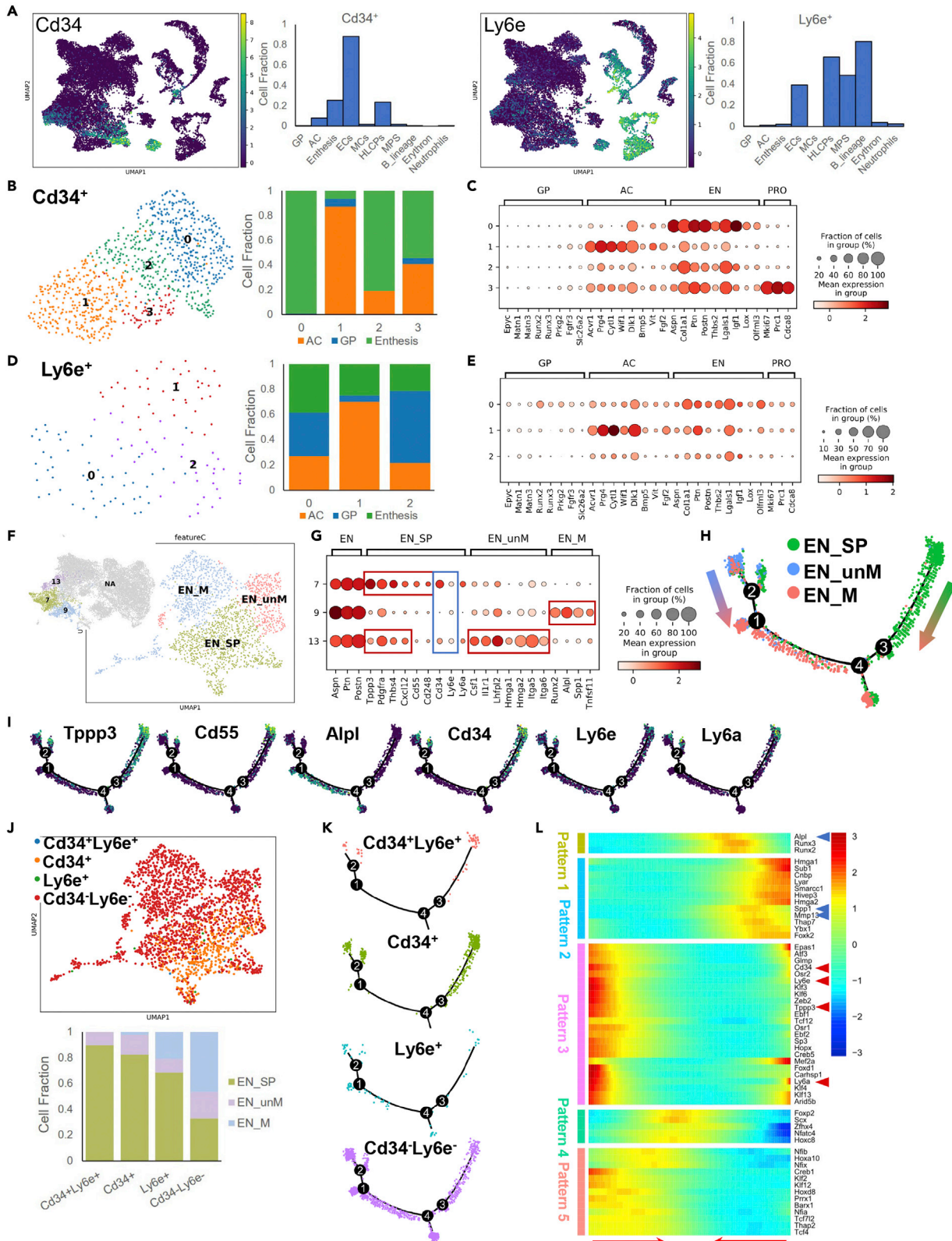


**Figure 4. Delineation of  $Cd34^+$  cell cluster and  $Ly6e^+$  cell cluster in enthesis cells**

- (A) UMAP plots showing expression patterns of  $Cd34$  and  $Ly6e$  in all delineated cells and fraction of the positive expressed cells in each cell type.
- (B) UMAP visualization of  $Cd34^+$  cells screened from AC, GP, and enthesis corresponding to Figure 2A revealing four subsets (Left) and fraction of cells from different cell types in each subset (Right).
- (C) Dot plots showing the expression of curated feature genes marked for GP, articular cartilage (AC), enthesis (EN), and cells in cell cycle (PRO) in each subset in (B) (Right).
- (D) UMAP visualization of  $Ly6e^+$  cells screened from AC, GP, and enthesis corresponding to Figure 2A revealing three subsets (Left) and fraction of cells from different cell types in each subset (Right).
- (E) Dot plots showing the expression of curated feature genes marked for GP, articular cartilage (AC), enthesis (EN), and cells in cell cycle (PRO) in each subset in (B) (Right).
- (F) UMAP visualization of enthesis cells revealing three subsets.
- (G) Dot plots showing feature genes expression of each subset in enthesis.
- (H) Pseudotime trajectory analysis of all subsets in enthesis predicted two major developmental branches with arrows indicating the predicted direction.
- (I) Distribution of cells expressing stem/progenitor marker genes (*Tppp3* and *Cd55*), terminal differentiation marker gene (*Alpl*), *Cd34*, *Ly6e*, and *Ly6a* along the pseudotime axis.
- (J) UMAP plots showing the distribution pattern of  $Cd34^+$  subset,  $Ly6e^+$  subset,  $Cd34^+Ly6e^+$  subset, and  $Cd34^-Ly6e^-$  subset in enthesis and the cell fraction distribution in different subset corresponding to F.
- (K) Pseudotime trajectory showing distribution of  $Cd34^+$  subset,  $Ly6e^+$  subset,  $Cd34^+Ly6e^+$  subset, and  $Cd34^-Ly6e^-$  subset.
- (L) Expression heatmap of curated TFs following pseudotime analysis displaying five clustering patterns with arrows indicating the predicted developmental direction corresponding to (H).

five distinct gene expression patterns (Figure 4L). Consistent with pseudotime trajectory analysis, two developmental lineages were observed, both of which began with active expression of *Tppp3*, *Cd34*, *Ly6e*, and *Ly6a*, which were clustered with stemness regulators such as *Klf* family, *Osr1/2*, *Zeb2*, *Foxd1*, *Hopx*, etc., as shown in pattern 3. In pattern 1 and 2, *Hmga1* and *Hmga2*, highly expressed in subset of EN\_unM, were clustered with TFs, which sequentially regulate joint development (*Cnbp* and *Smarcc1*),<sup>65,66</sup> chondrocyte differentiation (*Hivep3* and *Ybx1*),<sup>67,68</sup> and terminal differentiation (*Foxk2*, *Runx2*, and *Runx3*).<sup>69</sup> For the other developmental lineage shown in pattern 4 and 5, TFs regulating tendon development (*Scx*, *Foxp2*, *Nfact4*, etc.)<sup>70,71</sup> were gradually activated. These results suggested that  $Cd34^+$  and  $Ly6e^+$  cell subsets in enthesis could be candidate progenitors involving in enthesis development. Both of them contained heterogeneous subpopulations with differential lineage commitment of chondrocyte and tendon, suggesting involvement in the development of different zones of enthesis. Consistently, immunofluorescence staining of developing joint tissues showed that  $Cd34^+$  and  $Ly6e^+$  cells existed in the margin of articular cartilage, which extended to synovium and periosteum (Figures 3J and 3K).

**Distribution of  $Cd34$ ,  $Ly6e$ , and  $Ly6a$  in knee osteoarthritis**

Because of the heterogeneous features of  $Cd34^+$  subset and  $Ly6e^+$  subset, their pathological involvement in osteoarthritis was investigated. The immunofluorescence staining results showed that  $Cd34^+$  cells were activated in osteoarthritic cartilage, however distributed scattered in all zones but not restricted in surface zone, suggesting that  $Cd34^+$  subset played different roles in development and osteoarthritis (Figure S4A). *Ly6e*, co-expressed with *Ly6a* (Figure S4B), was pathologically activated at early stage of osteoarthritis and specifically gathered in edge of the affected articular cartilage and extended to synovium, which is a susceptible site to form osteophytes. As recently reported, osteophytes were derived from *Pdgfra*-expressing stem/progenitor cells, which would be activated during osteoarthritis.<sup>72</sup> However, our data (Figure 3I) and previous studies showed that *Pdgfra* was expressed broadly in joint tissues, including articular cartilage, tendon, and synovium,<sup>73–76</sup> and *Pdgfra*<sup>+</sup> cells showed high heterogeneity. In the contrary,  $Ly6e^+$  subset, also highly expressed *Pdgfra*, showed restricted distribution in the edge of articular cartilage, suggesting  $Ly6e^+$  subset as candidate progenitors specifically contributing to osteophyte formation in osteoarthritis.

**Interpretation of the cellular diversity and developmental progression of GP**

GP, landmark for limb endochondral bone development, is intricately composed but highly orchestrated, which also provides a vivid research model for both development and osteoarthritis. Therefore, we decoded the postnatal GP atlas reaching the interlinks with osteoarthritis. As shown before, nine subsets of GP chondrocytes were visualized (Figures S2A, S2B, and S5A). Based on the marker gene expression pattern, all subsets were integrated and clustered into 8 ones, including *Ptch1*<sup>+</sup>*Mki67*<sup>+</sup> subset and *Ptch1*<sup>+</sup> subset belonging to the proliferating zone in or out of the cell cycle (*Mki67*, *Ptch1*, *Pkdcc*, and *Slc26a2*),<sup>77–79</sup> pre-hypertrophic chondrocytes (preHC, *Wnt4*, *Panx3*, *Smpd3*, *Pth1r*, and *Ihh*),<sup>77,80–82</sup> *Col10a1*<sup>+</sup> hypertrophic chondrocytes (*Col10a1*<sup>+</sup>, *Col10a1*, and *Alpl*), *Spp1*<sup>+</sup> subset (*Spp1*, *Enpp1*, *Ank*,

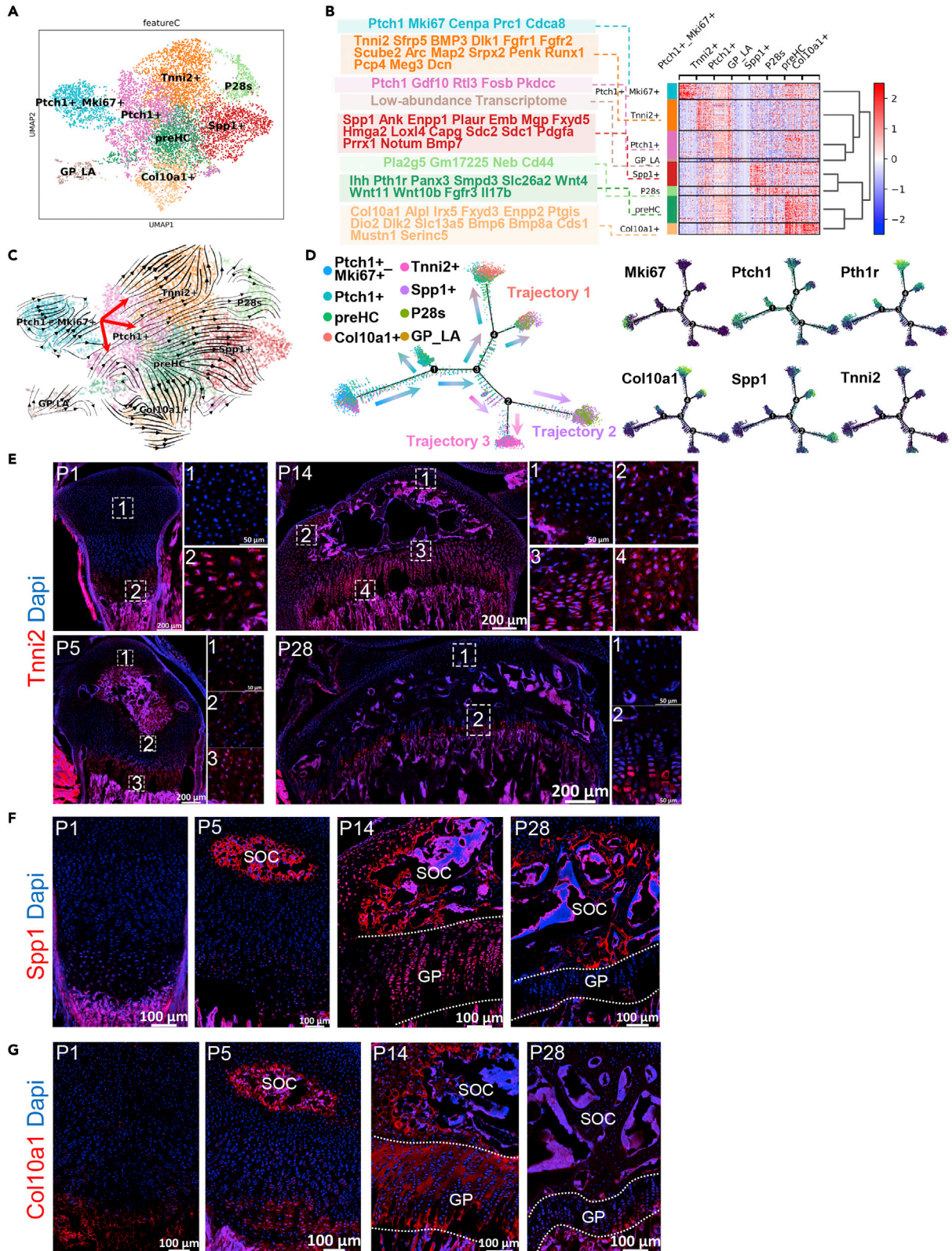


**Figure 5. Interpretation of the cellular diversity and developmental progression of postnatal GP chondrocytes**

(A) Identities of cells from GP (corresponding to Figure 2A) by UMAP visualization revealing eight cell types including *Ptch1*<sup>+</sup>*Mki67*<sup>+</sup> subset and *Ptch1*<sup>+</sup> subset belonging to the proliferating zone in or out of the cell cycle, pre-hypertrophic chondrocytes (preHC), *Col10a1*<sup>+</sup> hypertrophic chondrocytes (*Col10a1*<sup>+</sup>), *Spp1*<sup>+</sup> subset (*Spp1*<sup>+</sup>), *Tnni2*<sup>+</sup> subset (*Tnni2*<sup>+</sup>), one subset aggregated with cells derived from P28 (P28s), and the last one showing low abundance of transcriptome (GP\_LA).

(B) Heatmap denoting genes enriched in each type of cell subset.

(C) Developmental trajectory inferred by RNA velocity and visualized on the UMAP projection (corresponding to A) with arrows indicating three major predicted developmental branches.

(D) Pseudotime trajectory analysis of all subsets in GP predicted three major developmental branches with arrows indicating the predicted direction. Distribution of cells expressing feature genes along the pseudotime axis.

(E–G) Immunofluorescence staining of *Tnni2* (E), *Spp1* (F), and *Col10a1* (G) in GP of mice at P1, P5, P14, and P28 (n = 4 at each time point). Images of the boxed areas are shown on the right panels. Scale bars, 100 μm. Blue indicates DAPI staining of nuclei and red indicates *Tnni2*, *Spp1*, or *Col10a1* staining.

*Plaur*, and *Capg*), the newly discovered *Tnni2*<sup>+</sup> subset (*Tnni2*, *Sfrp5*, *Runx1*, *Penk*, and *Srpx2*), one subset aggregated with cells derived from P28 (P28s, *Cd44*, *Pla2g5*, etc.), and the last one exhibited low abundance of transcriptome (GP\_LA) (Figures 5A, 5B, S5B, and S5C). It seems counterintuitive that cells of *Spp1*<sup>+</sup> subset were not clustered with hypertrophic chondrocytes featured by *Col10a1*, although *Spp1* was generally recognized as a marker for terminal hypertrophic chondrocytes.<sup>83</sup> Actually, three developmental branches of *Tnni2*<sup>+</sup> subset, *Spp1*<sup>+</sup> subset, and *Col10a1*<sup>+</sup> subset were identified by RNA velocity analysis (Figure 5C) and pseudotime trajectory mapping (Figure 5D), which were all originated from proliferating chondrocytes. In addition, when mapping marker genes onto the pseudo-timeline, *Pth1r*, a marker for pre-hypertrophic chondrocytes and retarder of chondrocyte differentiation,<sup>84,85</sup> was restricted in trajectory 1 along with *Col10a1* (Figure 5D), suggesting that these branches went through different developmental progression. The above results revealed a more complicated cellular composition than recognized horizontal zones.<sup>86</sup>

In consideration of zonal re-arrangement and cell polarity regulation during SOC formation, the intermediate cells plotting in between articular cartilage and GP were analyzed by pseudotime trajectory (Figure S5D). It was unexpectedly indicated that mapping of the marker gene expression was slightly different with plotting of the specific subset, which showed that *Tnni2*, *Spp1*, and *Col10a1* were all highly expressed in the intermediate cells without plotting of *Col10a1*<sup>+</sup> subset. Further, it was revealed that *Col10a1* and *Spp1* were co-expressed at the downstream of each branch by marker gene expression embedded on UMAP visualization mapped with RNA velocity (Figure S5E). The above results suggested that each subset marked by *Tnni2*, *Spp1*, and *Col10a1* differentially evolved as GP developed, while co-expression of *Col10a1* and *Spp1* existed in certain stages of each subset. To assess the distribution of *Tnni2*, *Spp1*, and *Col10a1* in postnatal GP, we performed the immunofluorescence staining using murine limbs at different stages (Figures 5E–5G). *Tnni2* showed a spatiotemporally variational distribution during limb development (Figure 5E). At P1 without SOC development, *Tnni2* expressed mainly in the hypertrophic chondrocytes around the primary ossification center (POC). At P5 when the SOC starts formation, *Tnni2* increased the expression around SOC until P14, from which time point *Tnni2* declined expression in cells adjacent to articular cartilage. At P28 when the SOC gets mature, *Tnni2* was reduced in all cells around SOC but kept high expression in cells around POC. It was suggested that the spatiotemporal variation of *Tnni2*<sup>+</sup> cells seems related with the ossification center formation and maturation. *Spp1* was remarkably expressed around SOC as it develops, which showed a stronger signal than the expression adjacent to POC (Figure 5F). *Col10a1* was highly expressed in hypertrophic chondrocytes near both the POC and SOC, which was consistent with the previous reports (Figure 5G). Above all, each branch marked by *Tnni2*, *Spp1*, and *Col10a1* exhibited specific distribution pattern. Although both *Bmp3* and *Sfrp5* were previously recognized as resting zone markers,<sup>87</sup> the varied distribution of *Tnni2*<sup>+</sup> subset indicated more possibilities than resting cells.

To reveal the developmental progression of each branch, pseudotime trajectory of each subset was performed. Similar to the RNA velocity analysis (Figure S5E), *Col10a1* and *Spp1* were highly co-expressed at the terminal stage of every branch (Figure 6A). However, when screening the marker genes of late hypertrophic chondrocytes in each subset (Figure 6B), *Col10a1*<sup>+</sup> subset showed the most intensive expression. In the *Spp1*<sup>+</sup> subset, although a set of genes regulating pyrophosphate levels (*Ppa1*, *Enpp1*, *Ank*, and *Slc29a1*) were highly expressed, the lack of *Alpl* expression would retard the extracellular matrix mineralization,<sup>88</sup> which should not be the terminal state. To understand more accurately about the terminal state of hypertrophic chondrocytes, we screened out 7 independent subsets according to single-, dual-, or

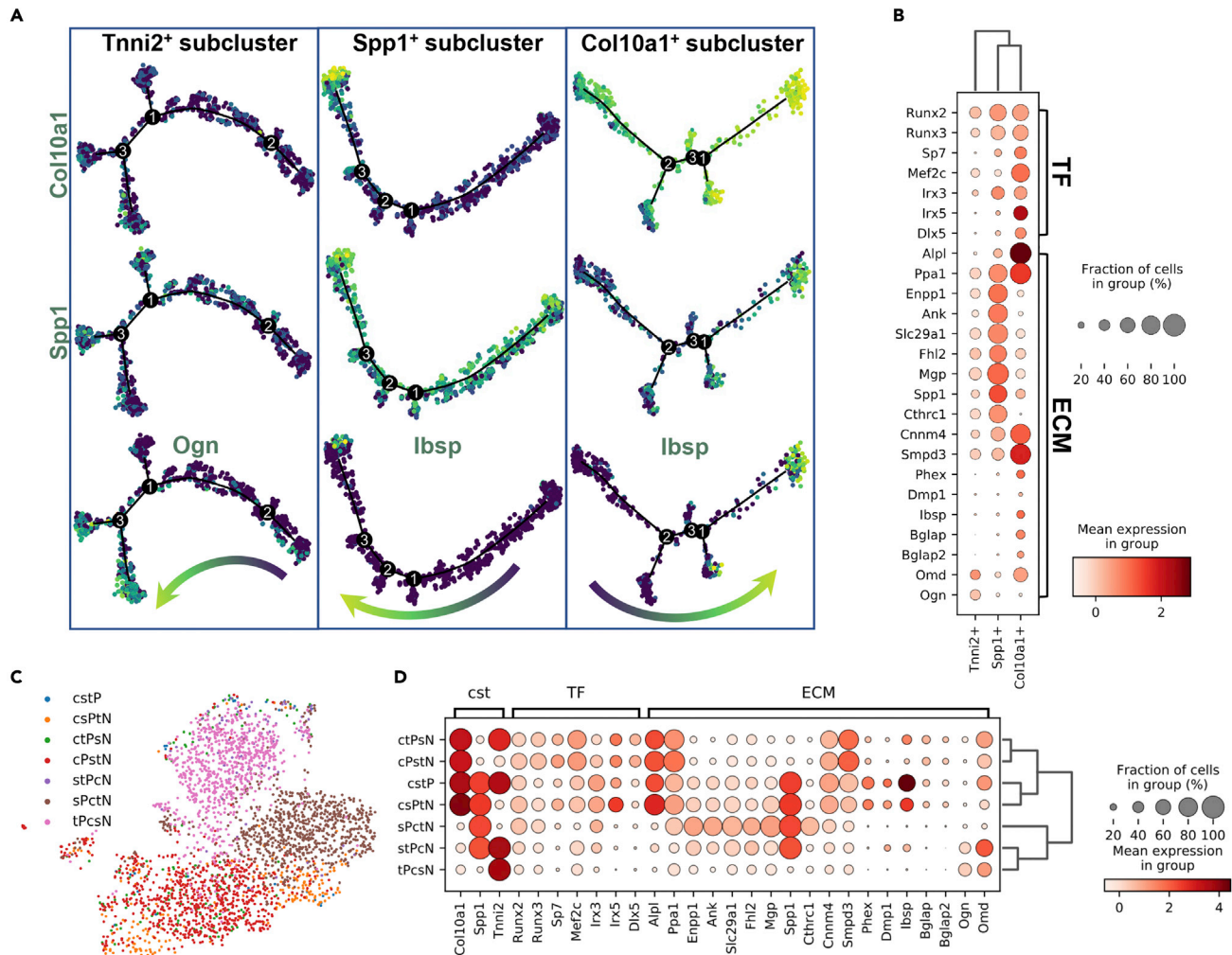


**Figure 6. Interpretation of the terminal stage of hypertrophic chondrocytes**

(A) Pseudotime trajectory analysis of *Tnni2*<sup>+</sup> subset, *Spp1*<sup>+</sup> subset, or *Col10a1*<sup>+</sup> subset, showing distribution of cells expressing feature genes along each pseudotime axis.

(B) Dot plots showing the curated feature genes expression regulating terminal differentiation and extracellular matrix mineralization in each branch.

(C) UMAP visualization of cells with single-, dual-, or triple-positive expression of *Tnni2*, *Spp1*, and *Col10a1*. cstP: *Tnni2*<sup>+</sup>*Spp1*<sup>+</sup>*Col10a1*<sup>+</sup> subset, csPtN: *Tnni2*<sup>+</sup>*Spp1*<sup>+</sup>*Col10a1*<sup>+</sup> subset, ctPsN: *Tnni2*<sup>+</sup>*Spp1*<sup>+</sup>*Col10a1*<sup>+</sup> subset, cPstN: *Tnni2*<sup>+</sup>*Spp1*<sup>+</sup>*Col10a1*<sup>+</sup> subset, stPcN: *Tnni2*<sup>+</sup>*Spp1*<sup>+</sup>*Col10a1*<sup>-</sup> subset, sPctN: *Tnni2*<sup>+</sup>*Spp1*<sup>+</sup>*Col10a1*<sup>-</sup> subset, tPcsN: *Tnni2*<sup>+</sup>*Spp1*<sup>-</sup>*Col10a1*<sup>-</sup> subset.

(D) Dot plots showing curated feature genes expression regulating terminal differentiation and extracellular matrix mineralization in each subset corresponding to (C).

triple-positive expression of *Col10a1*, *Spp1*, and *Tnni2* (Figures 6C and S5G). The *Col10a1*<sup>+</sup>*Spp1*<sup>+</sup> subsets (cstP and csPtN) were indicated as the late hypertrophic chondrocytes with extensive expression of *Runx2*, *Sp7*, *Irx3*, *Irx5*, *Alpl*, *Ibsp*, etc. Although the TFs regulating terminal differentiation were also expressed in *Col10a1*<sup>+</sup>*Spp1*<sup>-</sup> subsets (ctPsN and cPstN), the extracellular matrix was likely unmineralized based on low expression of *Ibsp*. Nonetheless, the expression level of *Tnni2* made little difference to the terminal state (Figure 5D). Therefore, it could be established that the double positive expression of *Col10a1* and *Spp1* could mark the terminal differentiated hypertrophic chondrocytes, which was in consistent with the immunofluorescence staining results (Figures 5E–5G).

To understand the main features of each subset, the expression pattern of key regulating factors was inspected, including signaling factors (Figure S6A) and TFs (Figure S6H). Interestingly, apparently disparate regulating patterns were displayed among each subset. Thereinto, the *Tnni2*<sup>+</sup> subset showed

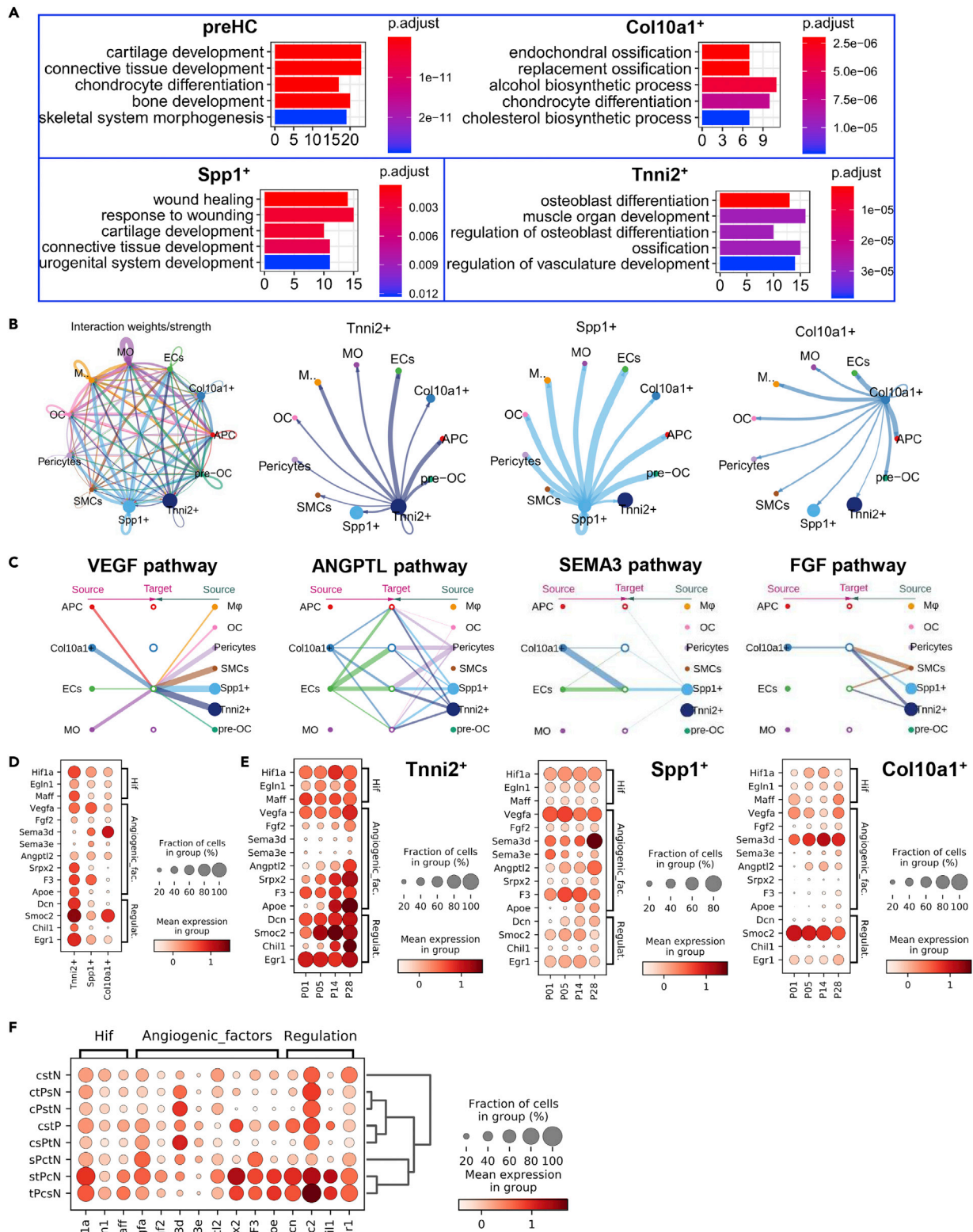


**Figure 7. Biological pathways of each developmental branch in GP**

(A) GO analysis showing enriched BP terms in each subset of GP.

(B) Circle plot showing the overall intercellular communication network or in specific subset inferred by CellChat. Circle sizes were proportional to the number of cells in each cell group and edge width represented the communication probability. Edge colors represented different cell subset.

(C) Hierarchical plot showing interactions among different cell subsets via angiogenic-related signaling pathways, including *Vegf*, *Angptl*, *Sema3*, and *Fgf* signaling pathway. Circle sizes were proportional to the number of cells in each cell group and edge width represented the communication probability.

(D and E) Dot plots showing the expression of curated genes regulating angiogenesis in each developmental branch of GP (D) or at different developmental stages in specific branch (E).

(F) Dot plots showing the expression of curated genes regulating angiogenesis in each subset with single-, dual-, or triple-positive expression of *Tnni2*, *Spp1*, and *Col10a1* in GP (corresponding to Figure 6C).

coincident inhibition of *Bmp* (*Bmp3*) and *Wnt* (*Sfrp5*)<sup>89,90</sup> with terminal differentiation (Figures S6B and S6C). High expression of *Bmp3*, an inhibitor of chondrocyte maturation, could explain the lack of *Ibsp* expression even in the late stage of *Tnni2*<sup>+</sup> subset. The *Spp1*<sup>+</sup> subset exhibited *Bmp* activation (increased *Bmp7* and decreased *Inhba*) but *Wnt* inhibition (decreased *Wnt7b* and increased *Notum*) (Figures S6D and S6E). Unlike the other *Bmp* ligands, *Bmp7* was reported suppressing hypertrophic differentiation,<sup>91</sup> and *Wnt7b* oppositely functioned in inducing chondrocyte maturation.<sup>92</sup> As a result, the terminal differentiation of *Spp1*<sup>+</sup> subset was restricted. The *Col10a1*<sup>+</sup> subset showed intense *Bmp* activation (increased *Bmp2*, *Bmp6*, and *Bmp8a*, and decreased *Chrdl1*) and *Wnt* inhibition (decreased *Wnt4*, *Wnt10b*, and *Wnt11*, and increased *Frzb*), concentrically leading to chondrocyte terminal differentiation. Similarly, the TFs highly expressed in each subset were specific. Along with *Tnni2*<sup>+</sup> subset terminal differentiation, *Runx1* and *Mef2c* were up-regulated (Figure S6I). In the *Spp1*<sup>+</sup> subset, the recognized TFs regulating chondrocyte terminal differentiation, including *Runx2* and *Runx3*,<sup>93</sup> *Irx3* and *Irx5*,<sup>94</sup> *Sp7* and *Mef2c*,<sup>95</sup> were predominantly up-regulated at the terminal stage (Figure S7J). Most of the TFs highly expressed in the *Spp1*<sup>+</sup> subset exhibited more extensive distribution along with the trajectory of *Col10a1*<sup>+</sup> subset (Figure S6K). In spite of the similarities between *Spp1*<sup>+</sup> subset and *Col10a1*<sup>+</sup> subset, critical different regulating factors decided their specificity. *Runx3*, reported down-regulation at late hypertrophic chondrocytes,<sup>93</sup> was down-regulated in the *Col10a1*<sup>+</sup> subset but up-regulated at terminal stage of the *Spp1*<sup>+</sup> subset, which was probably a switch controlling the terminal state of hypertrophic chondrocyte. In addition, *Irx3* and *Irx5* were reported promoting osteogenesis of hypertrophic chondrocytes as downstream of *Wnt* signaling,<sup>94</sup> while plotted at different stages of *Spp1*<sup>+</sup> subset and *Col10a1*<sup>+</sup> subset. By plotting the subsets with positive expression of *Col10a1*, *Spp1*, and *Tnni2* on pseudotime trajectory, it was shown that *Irx3* was expressed mainly in the *Spp1*<sup>+</sup> subset and *Irx5* was expressed mainly in the *Col10a1*<sup>+</sup> subset (Figure S6L), suggesting their specific roles on regulating differentiation of each subset. Above all, each developmental cell branch was specifically regulated by key factors. Next, we discuss the potential biological functions of each branch in inducing endochondral bone development.

**Biological functions of each developmental branch of GP**

Vascularization coordinated by hypertrophic chondrocytes during endochondral bone development has been well studied.<sup>96</sup> However, as mentioned above, different branches of GP chondrocytes could develop into terminal hypertrophic chondrocytes, yet their contribution to vascularization was unclear. GO enrichment analysis identified that the *Tnni2*<sup>+</sup> subset was highlighted in regulating vascularization (Figure 7A). To reveal the global communications between each branch of GP chondrocytes and ECs, the receptor-ligand database was established by CellChat.<sup>97</sup> The *Tnni2*<sup>+</sup> subset and *Spp1*<sup>+</sup> subset showed intensive receptor-ligand communications with ECs (Figure 7B). For the inferred angiogenic pathways, the *Vegf* (*Vegfa-Vegfr1/Vegfr2*) and *Angptl* pathways (*Angptl2-Itga5/Itgb1*) was comparatively active in each subset, the *Sema3* pathway was primarily active in the *Col10a1*<sup>+</sup> subset (*Sema3d-Nrp1/Plxna2*), and the *Fgf* pathway was most active in the *Tnni2*<sup>+</sup> subset (*Fgf2-Fgfr1*) (Figure 7C). In addition, regulators of angiogenesis were identified in the highly differentially expressed genes, including *Hif-1α* signaling factors, angiogenic factors, and other regulators. The *Tnni2*<sup>+</sup> subset revealed the most intense and gradually increased expression of the above genes, except for *Sema3d* (Figures 7D and 7E). In the *Spp1*<sup>+</sup> subset, *Vegfa*, *Sema3d*, and *F3* were prominently expressed, of which *Sema3d* showed increased expression at P28 (Figures 7D and 7E). In the *Col10a1*<sup>+</sup> subset, *Sema3d* and *Smoc2* were highly expressed, with a stable expression level during development (Figures 7D and 7E). Furthermore, in subsets with different marker gene expression, the *Tnni2*<sup>+</sup> subset and *Spp1*<sup>+</sup> *Tnni2*<sup>+</sup> subset revealed predominant expression of the above angiogenic regulators (Figure 7F).

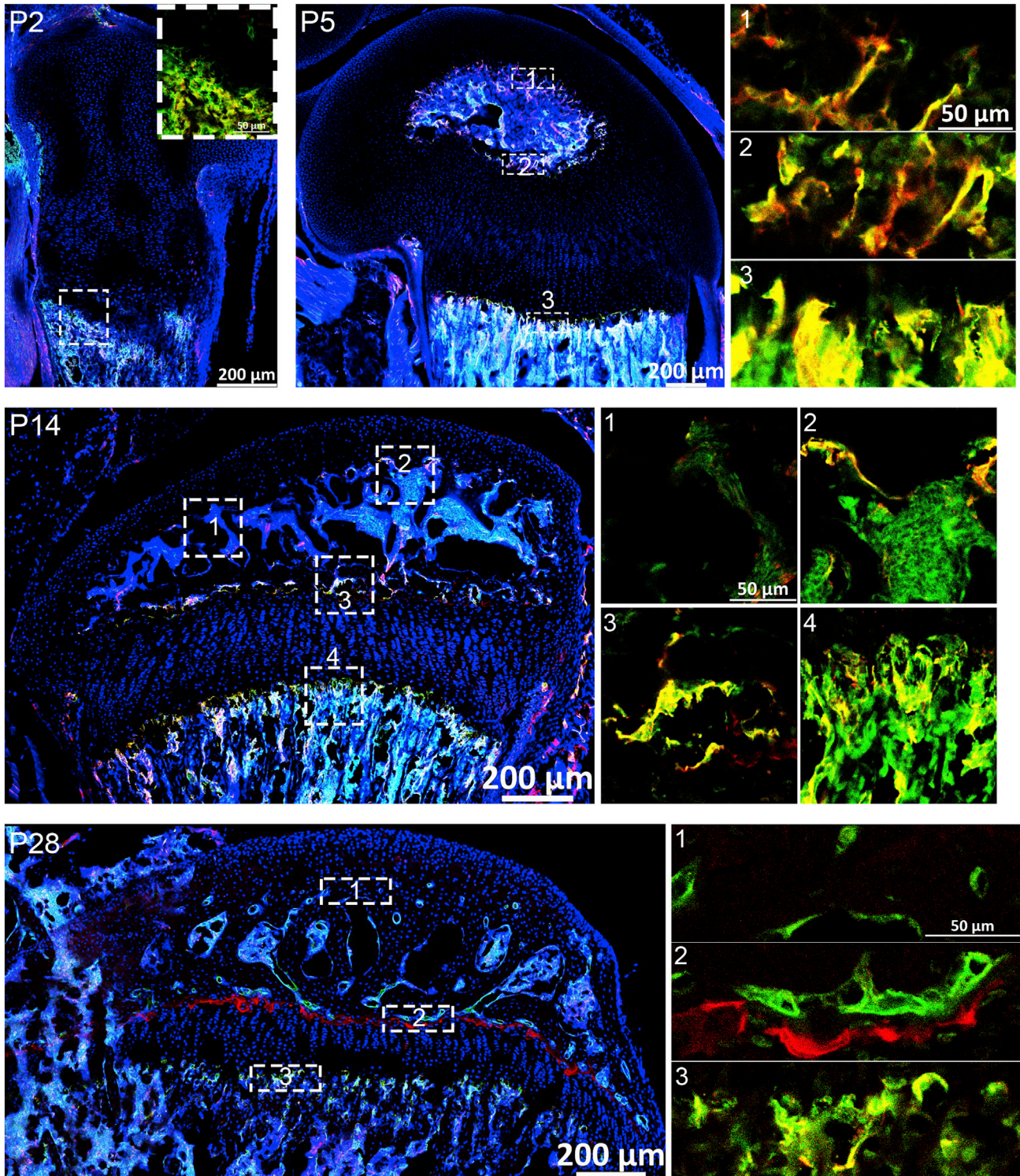


**Figure 8. Distribution of  $Cd31^hEmcn^h$  vessels in murine postnatal hind limbs**

Co-immunofluorescence staining of  $Cd31$  and  $Emcn$  in murine hind limbs at different postnatal stages, including P2, P5, P14, and P28 ( $n = 4$  at each time point). Images of the boxed areas are shown on the right panels. Blue indicates DAPI staining of nuclei, red indicates  $Cd31$  staining, and green indicates  $Emcn$  staining. Scale bars, 200  $\mu m$ .

To discuss the correlation with vascularization, the distribution pattern of each subset and the type H vessels were detected (Figure 8). Results showed that at P2, the  $Cd31^hEmcn^h$  vessels distributed in POC and emerged in the surrounding area of SOC at P5. At P14, the  $Cd31^hEmcn^h$  vessels gradually decreased in the lateral area of SOC adjacent to the articular cartilage and continued decreased in all surrounding areas of the SOC at P28. The distribution pattern of  $Cd31^hEmcn^h$  vessels was similar to the one of  $Tnni2$ . Therefore, we proposed the  $Tnni2^+$  subset as being key in inducing angiogenesis of the postnatal endochondral bone, especially of the SOC.

### Distribution of *Tnni2* and *Spp1* in articular cartilage during osteoarthritis progression

Chondrocyte terminal differentiation is a landmark for endochondral bone development as well as cartilage degeneration in osteoarthritis. Research of postnatal GP development also provides a potential model for exploring the pathomechanisms of osteoarthritis. With continuation of the above results, we explored the distribution of *Tnni2* and *Spp1* in osteogenic joint. Immunofluorescence staining showed that the expression of *Tnni2* increased during early osteoarthritis but gradually decreased later (Figure S7A). In contrast, the expression of *Spp1* steadily increased with osteoarthritis progression (Figure S7B). Similar to postnatal limb development, *Tnni2* was transiently highly expressed, while *Spp1* expression gradually increased, suggesting each pathological contribution at different osteoarthritis stages.

## DISCUSSION

As a connector of tissue morphogenesis and maturation, postnatal developmental stage is one important part of developmental biology. Postnatal limb development is one sophisticated system orchestrated with different types of tissue organization, maturation, and remodeling. In articular cartilage, chondrocytes perform zonal organization and maturation during postnatal stage,<sup>98</sup> accompanied with losing of the self-renewing ability.<sup>99</sup> In GP, all cellular stages would be observed from postnatal skeletal stem cells<sup>8</sup> to terminal and mineralized chondrocytes. In addition, specific cellular biological clues could be provided by the occurrence of SOC in murine postnatal limbs, when the articular cartilage and subchondral bone develop, mature, and separate from one entire cartilage template.

In embryonic stage, the articular cartilage is developed from joint progenitor cells located in the intermediate compartment of the histological interzone, which is broadly labeled by Gdf5.<sup>98,100</sup> Over postnatal life, it is evidenced that embryonically derived progenitors remain present while dramatically decreased in articular cartilage.<sup>101–103</sup> In adult articular cartilage, cell populations with progenitor or stem character are also discovered in the superficial zone.<sup>10,11</sup> Although it was verified that human superficial chondrocytes showed proliferative remodeling of the spatial organization in response to distant lesions of early osteoarthritis<sup>104</sup> and synovial *Prg4*<sup>+</sup> lineage progenitors at prenatal or juvenile stages contributed to repairment of adult articular cartilage injury,<sup>103</sup> the intrinsic regenerative capacity of articular cartilage is quite limited once it has reached maturity.<sup>105,106</sup> By contrast, the juvenile articular cartilage was verified possessing potent self-repair potential.<sup>99</sup> In addition, the super-healing MRL mouse strain had a remarkable healing response of damaged cartilage with more abundant chondrocytes and a richer extracellular matrix compared with non-healer strains.<sup>107,108</sup> And genes activating cell proliferation were discovered highly expressed in the super-healing mouse strains, which was correlated with the enhanced articular cartilage self-repair.<sup>108,109</sup> Above all, alterations of stem or progenitor cell pool at postnatal stage could be attributed to the declined regenerative capability.<sup>110</sup> In the present study, the systematic mapping of AC during postnatal development is valuable for revealing the transition of its intrinsic repair capacity.

In the present study, two sub-clusters of candidate articular cartilage progenitors featured by *Cd34* or *Ly6e/Ly6a* were discovered. *Cd34* was first described on hematopoietic stem and progenitor cells,<sup>111</sup> and recently, considerable studies have demonstrated that *Cd34* is expressed by a multitude of other non-hematopoietic cell types including fibrogenic/adipogenic progenitors,<sup>112</sup> muscle satellite cells,<sup>113</sup> corneal keratocytes, interstitial cells, epithelial progenitors, and vascular endothelial progenitors.<sup>114</sup> It shows that *Cd34*<sup>+</sup> cells discovered in various tissues are usually characterized with enhanced progenitor features. Therefore, it was exciting to detect *Cd34*<sup>+</sup> cells in developmental articular cartilage. The transcriptome features and surface-zone distribution pattern indicated *Cd34*<sup>+</sup> chondrocytes as the articular cartilage progenitors. Interestingly, we detected that *Cd34*<sup>+</sup> chondrocytes arose after joint morphogenesis, which suggested the sub-cluster as a candidate progenitor subset contributing to postnatal articular cartilage development. Similarly, *Ly6e*<sup>+</sup> cells, co-expressed with *Ly6a*, were transcriptionally characterized as progenitors. However, unlike *Cd34*<sup>+</sup> chondrocytes, *Ly6e*<sup>+</sup> cells were distributed mainly on the margin of

articular cartilage with interconnection to the synovium, which suggested their distinct roles on articular cartilage development. However, before we make any conclusions, more precise experiments should be carried out especially using the lineage tracing mice models.

Interestingly, during entheses development, both  $Cd34^+$  cells and  $Ly6e^+$  cells were characterized with two developmental lineages of mineralized chondrocyte and tendon. As a transitional fibrocartilaginous tissue between tendon and bone, entheses occurs postnatally<sup>115,116</sup> and forms four distinct zones that create a structurally continuous gradient from tendon, fibrocartilage, and calcified fibrocartilage to bone.<sup>117–119</sup> Besides the newly discovered progenitors marked by  $Cd34$  and  $Ly6e$ , all the recognized progenitors marked by  $Tppp3$ ,  $Cd55$ , and  $Cd247$  developed into two trajectories. In addition, all the above marker genes were remarkably co-expressed in the progenitors of entheses. Therefore, unlike the situation in postnatal articular cartilage with distinct progenitor subsets, the progenitors of entheses showed multilineage potential while with similar marker gene expression.

During osteoarthritis progression, both  $Cd34^+$  cells and  $Ly6e^+$  cells were pathologically activated in articular cartilage.  $Cd34^+$  cells showed scattered distribution at all zones rather than surface-zone distribution, while  $Ly6e^+$  cells were intensively distributed in margin of articular cartilage, the susceptible sites for osteophytes. Previously, Roelofs et al. reported that osteophytes were derived from  $Pdgfra$ -expressing stem/progenitor cells in periosteum and synovium.<sup>72</sup> However,  $Pdgfra$  is widely expressed in the developing joint with a considerable heterogeneity.<sup>74</sup> Our results indicated that  $Ly6e^+$  cells were also a sub-cluster of  $Pdgfra$ -expressing cells. Based on the particularly restrictive distribution pattern,  $Ly6e^+$  cells were likely the specific subset contributing to osteophyte formation. To clearly define the responsible pathological subset would expedite understanding of the pathomechanisms and stimulate promising treatment strategies. Therefore, deeper exploration is required to figure out the roles and regulating mechanisms of  $Cd34^+$  cells and  $Ly6e^+$  cells in both joint development and degenerative diseases.

In GP, three developmental branches marked by  $Tnni2$ ,  $Spp1$ , and  $Col10a1$  were interpreted in the present study. Conventionally, the knowledge of five-zone organization in GP cartilage has been established, which develops through a linear sequence from resting chondrocytes to terminally mineralized hypertrophic chondrocytes.<sup>8,9,120</sup> The linear sequential developmental theory explains how long bones achieve elongation, contributed by proliferation of GP chondrocytes, increase of cell volume, deposition of extracellular matrix, and at last coordination with bone formation,<sup>120</sup> which occurs mainly in POC. However, this theory is probably no longer fully applicable in postnatal stage concerning with SOC formation, which shows significantly developmental difference compared with POC. For example, as soon as SOC develops, the underlying chondroprogenitors start to renew themselves making contribution to the elongation of POC while influenced by SOC.<sup>8,9</sup> Therefore, it is suggested that these chondroprogenitors are named as “epiphyseal stem cells” and SOC as “epiphyseal stem cell niche,”<sup>121</sup> indicating key developmental difference between POC and SOC. Nowadays, it is still largely unclear about the SOC developmental pattern, roles, and regulating mechanisms.

During postnatal limb development, the formation of SOC separates articular cartilage and GP into two distinct structures.<sup>7</sup> As reported, SOC evolutionarily appears in animals conquering the land—amniotes, which correlates with the extent of mechanical loads and probably protect the GP from the high mechanical stress encountered in the terrestrial environment.<sup>7,122</sup> Consistently, subchondral bone, developmentally derived from SOC, is reported with similar bone mineral density with cortical tibial metaphysis, which is higher than the POC-derived cancellous metaphysis.<sup>123</sup> The same happened to the epiphyseal bone plate, a flat bony structure located between the epiphysis and the metaphysis of the long bones that provides strength and firmness to the GP cartilage.<sup>124</sup> Considered together, rather than elongation, the development of SOC is more focused on the extracellular matrix mineralization to reinforce the mechanical properties. In the present study, we discovered that cells around the SOC showed remarkably higher expression of  $Spp1$  than cells adjacent to the POC, although both areas of cells expressed similar levels of  $Col10a1$ . The  $Col10a1^+Spp1^+$  subset expresses highest levels of terminal differentiation marker genes and extracellular matrix mineralization regulating genes; however, higher expression of  $Spp1$  may indicate increased bone mineral density and strengthened mechanical properties. These findings are valuable for studies in controlling artificial bone density.

What is even more surprising is that the newly discovered  $Tnni2^+$  subset, rather than  $Col10a1^+$  subset, showed the most powerful effect of promoting angiogenesis.  $Tnni2^+$  cells showed distinctive distribution

changes, which seems related to the developmental activity of ossification centers. Consistently, type H vessels, coupling of angiogenesis and osteogenesis in bone,<sup>19</sup> exhibited similar variation with *Tnni2*<sup>+</sup> cells in POC and SOC. The above results suggest that *Tnni2*<sup>+</sup> GP chondrocytes may bridge type H vessels with ossification centers during endochondral bone formation.

GP is also an elegant experimental model to study chondrocyte terminal differentiation, which is common in articular cartilage degenerative diseases including osteoarthritis. As a disease of mechanics, typical degenerative progression during osteoarthritis includes cartilage erosion, subchondral bone structure alteration, osteophyte formation, destruction of osteochondral junction, synovial hyperplasia, and systemic aseptic inflammation.<sup>106,125–127</sup> Thereinto, chondrocyte hypertrophic change would accelerate cartilage deterioration by inducing extracellular matrix degradation and calcification, vascular invasion, nerve innervation, and inflammation,<sup>128–131</sup> the cellular biological process of which is similar to endochondral bone development.<sup>132–134</sup> In the present study, we interpreted the key regulators differentially expressed in the AC and GP chondrocytes, which provided more biological clues to maintain chondrocyte homeostasis. Moreover, similar to the spatial-temporal evolutionary pattern in GP development, *Tnni2* showed transiently high expression in the early stage of osteoarthritic cartilage, while the expression of *Spp1* gradually increased with osteoarthritis progression. These findings are helpful in deeply understanding the pathomechanisms of osteoarthritis. Yet, many unanswered questions remained, such as do lineage connections exist among different branches, whether and how the *Tnni2*<sup>+</sup> subset induced vascularization in GP and osteoarthritic cartilage, and what regulators are shared in regulating each branch differentiation in GP development and osteoarthritis.

In conclusion, interpretation of articular cartilage progenitors and GP developmental branches in this study expanded the horizon of our knowledge about postnatal limb development. Reaching the inter-connections between postnatal limb development and osteoarthritis progression broadens our understanding about the pathomechanisms, which might stimulate promising treatment strategies in the future.

### Limitations of the study

This study is mainly based on high-throughput scRNA-seq technique, showing abundant information on the gene expression during the postnatal limb development. However, two major limitations should be considered in the interpretation of the results. First, the bioinformatic analysis is thorough but lacks integrated validation. *Cd34*<sup>+</sup> cell subset and *Ly6e*<sup>+</sup> cell subset in articular cartilage and enthesis are suggested as candidate progenitors based on the transcriptome features and distribution patterns. However, more functional and lineage tracing experiments should be performed to explicit the properties of these cell subsets. Similarly, three cellular developmental branches are interpreted in GP chondrocytes. Each branch shows specific transcriptome features and distribution patterns while with connections as terminal differentiation. Yet, the lineage specificity and connections among different branches and the biological functions of each subset need more exploration in the future. Second, it is difficult to highlight the inter-connections between postnatal limb development and osteoarthritis progression simply by observing the distribution of the annotated cell subsets in osteoarthritis mice. Co-analysis of scRNA-seq data from postnatal limbs and osteoarthritic articular cartilage, functional experiments, and lineage tracing in osteoarthritis mouse models are all required to lead to the identification of intrinsic connections between limb development, remodeling, and regeneration.

### STAR★METHODS

Detailed methods are provided in the online version of this paper and include the following:

- [KEY RESOURCES TABLE](#)
- [RESOURCE AVAILABILITY](#)
  - Lead contact
  - Materials availability
  - Data and code availability
- [EXPERIMENTAL MODEL AND SUBJECT DETAILS](#)
  - Animals
- [METHOD DETAILS](#)
  - Preparation of single-cell suspension
  - Construction of scRNA-seq libraries, quality control, and sequencing
  - Processing of scRNA-seq data

- Limb tissue preparation and cryosection
- Immunofluorescent staining
- QUANTIFICATION AND STATISTICAL ANALYSIS

## SUPPLEMENTAL INFORMATION

Supplemental information can be found online at <https://doi.org/10.1016/j.isci.2022.105808>.

## ACKNOWLEDGMENTS

The present study was supported by the National Natural Science Foundation of China (31900583, U22A20162, 32071351, 81772400), the Natural Science Foundation of Guangzhou City (201807010031), foundation of Shenzhen Committee for Science and Technology Innovation (JCYJ20190809142211354, GJHZ20180929160004704, JCYJ20210324102607021), Sanming Project of Medicine in Shenzhen (SZSM201911002), the Beijing Municipal Health Commission (Grant No. BMHC-2021-6, BMHC-2019-9, BMHC-2018-4, PXM2020\_026275\_000002), AOCMF Translational approaches for bone constructs CPP (AOCMF-21-04S), and Sun Yat-sen University Clinical Research 5010 Program (No. 2019009). We would like to thank Accuramed Technology (Shanghai) Limited (<https://www accuramed.com/>) for the technical supports of the scRNA-seq (10x Single Cell sequencing), and special thanks are extended to Guangxu Zhang and Ruijuan Cheng for technical support.

## AUTHOR CONTRIBUTIONS

Conceptualization: M.M.G. and Z.Y.Z.; Methodology: M.M.G., Z.Y.Z., and X.N.Z.; Investigation: M.M.G., Z.Y.Z., X.Z.L., P.G., J.M.W., J.H.L., W.T.W., B.L.L., H.C.W., Z.Y.H., and S.Y.L.; Writing – Original draft: M.M.G. and Z.Y.Z.; Writing – Review and editing: M.M.G., Z.Y.Z., X.N.Z., M.S., S.G., and Z.L.; Supervision: Z.Y.Z., X.N.Z., D.F.C., and W.M.Z.; Funding acquisition: Z.Y.Z., S.Y.L., D.F.C., W.M.Z., and M.M.G.

## DECLARATION OF INTERESTS

The authors declare no competing interests.

## INCLUSION AND DIVERSITY

We support inclusive, diverse, and equitable conduct of research.

Received: February 12, 2022

Revised: August 22, 2022

Accepted: December 9, 2022

Published: January 20, 2023

## REFERENCES

1. He, J., Yan, J., Wang, J., Zhao, L., Xin, Q., Zeng, Y., Sun, Y., Zhang, H., Bai, Z., Li, Z., et al. (2021). Dissecting human embryonic skeletal stem cell ontogeny by single-cell transcriptomic and functional analyses. *Cell Res.* 31, 742–757. <https://doi.org/10.1038/s41422-021-00467-z>.
2. McQueen, C., and Towers, M. (2020). Establishing the pattern of the vertebrate limb. *Development* 147, dev177956. <https://doi.org/10.1242/dev.177956>.
3. Serrano, N., and O'Farrell, P.H. (1997). Limb morphogenesis: connections between patterning and growth. *Curr. Biol.* 7, R186–R195. [https://doi.org/10.1016/s0960-9822\(97\)70085-x](https://doi.org/10.1016/s0960-9822(97)70085-x).
4. Petit, F., Sears, K.E., and Ahituv, N. (2017). Limb development: a paradigm of gene regulation. *Nat. Rev. Genet.* 18, 245–258. <https://doi.org/10.1038/nrg.2016.167>.
5. Gerber, T., Murawala, P., Knapp, D., Masselink, W., Schuez, M., Hermann, S., Gac-Santel, M., Nowoshilow, S., Kageyama, J., Khattak, S., et al. (2018). Single-cell analysis uncovers convergence of cell identities during axolotl limb regeneration. *Science* 362, eaag0681. <https://doi.org/10.1126/science.aag0681>.
6. Lu, P., Takai, K., Weaver, V.M., and Werb, Z. (2011). Extracellular matrix degradation and remodeling in development and disease. *Cold Spring Harbor Perspect. Biol.* 3, a005058. <https://doi.org/10.1101/cshperspect.a005058>.
7. Xie, M., and Chagin, A.S. (2021). The epiphyseal secondary ossification center: evolution, development and function. *Bone* 142, 115701. <https://doi.org/10.1016/j.bone.2020.115701>.
8. Mizuhashi, K., Ono, W., Matsushita, Y., Sakagami, N., Takahashi, A., Saunders, T.L., Nagasawa, T., Kronenberg, H.M., and Ono, N. (2018). Resting zone of the growth plate houses a unique class of skeletal stem cells. *Nature* 563, 254–258. <https://doi.org/10.1038/s41586-018-0662-5>.
9. Newton, P.T., Li, L., Zhou, B., Schweingruber, C., Hovorakova, M., Xie, M., Sun, X., Sandhow, L., Artemov, A.V., Ivashkin, E., et al. (2019). A radical switch in clonality reveals a stem cell niche in the epiphyseal growth plate. *Nature* 567, 234–238. <https://doi.org/10.1038/s41586-019-0989-6>.
10. Alsalameh, S., Amin, R., Gemba, T., and Lotz, M. (2004). Identification of mesenchymal progenitor cells in normal and osteoarthritic human articular cartilage. *Arthritis Rheum.* 50, 1522–1532. <https://doi.org/10.1002/art.20269>.
11. Dowthwaite, G.P., Bishop, J.C., Redman, S.N., Khan, I.M., Rooney, P., Evans, D.J.R.,

- Haughton, L., Bayram, Z., Boyer, S., Thomson, B., et al. (2004). The surface of articular cartilage contains a progenitor cell population. *J. Cell Sci.* *117*, 889–897. <https://doi.org/10.1242/jcs.00912>.
12. Rikkers, M., Korpershoek, J.V., Levato, R., Malda, J., and Vonk, L.A. (2022). The clinical potential of articular cartilage-derived progenitor cells: a systematic review. *NPJ Regen. Med.* *7*, 2. <https://doi.org/10.1038/s41536-021-00203-6>.
13. Nagy, A., Kénesi, E., Rentsendorj, O., Molnár, A., Szénási, T., Sinkó, I., Zvara, A., Oommen, S.T., Barta, E., Puskás, L.G., et al. (2011). Evolutionarily conserved, growth plate zone-specific regulation of the matrilin-1 promoter: L-Sox5/Sox6 and Nfi factors bound near TATA finely tune activation by Sox9. *Mol. Cell Biol.* *31*, 686–699. <https://doi.org/10.1128/mcb.00019-10>.
14. Wilson, R., Norris, E.L., Brachvogel, B., Angelucci, C., Zivkovic, S., Gordon, L., Bernardo, B.C., Stermann, J., Sekiguchi, K., Gorman, J.J., and Bateman, J.F. (2012). Changes in the chondrocyte and extracellular matrix proteome during post-natal mouse cartilage development. *Mol. Cell. Proteomics* *11*, M111.014159. <https://doi.org/10.1074/mcp.M111.014159>.
15. Lui, J.C., Chau, M., Chen, W., Cheung, C.S.F., Hanson, J., Rodriguez-Canales, J., Nilsson, O., and Baron, J. (2015). Spatial regulation of gene expression during growth of articular cartilage in juvenile mice. *Pediatr. Res.* *77*, 406–415. <https://doi.org/10.1038/pr.2014.208>.
16. Jeon, J., Oh, H., Lee, G., Ryu, J.H., Rhee, J., Kim, J.H., Chung, K.H., Song, W.K., Chun, C.H., and Chun, J.S. (2011). Cytokine-like 1 knock-out mice (Cyt1<sup>-/-</sup>) show normal cartilage and bone development but exhibit augmented osteoarthritic cartilage destruction. *J. Biol. Chem.* *286*, 27206–27213. <https://doi.org/10.1074/jbc.M111.218065>.
17. Kuntz, L.A., Rossetti, L., Kunold, E., Schmitt, A., von Eisenhart-Rothe, R., Bausch, A.R., and Burgkart, R.H. (2018). Biomarkers for tissue engineering of the tendon-bone interface. *PLoS One* *13*, e0189668. <https://doi.org/10.1371/journal.pone.0189668>.
18. Kult, S., Olender, T., Osterwalder, M., Markman, S., Leshkowitz, D., Krief, S., Blecher-Gonen, R., Ben-Moshe, S., Farack, L., Keren-Shaul, H., et al. (2021). Bi-fated tendon-to-bone attachment cells are regulated by shared enhancers and KLF transcription factors. *Elife* *10*, e55361. <https://doi.org/10.7554/eLife.55361>.
19. Kusumbe, A.P., Ramasamy, S.K., and Adams, R.H. (2014). Coupling of angiogenesis and osteogenesis by a specific vessel subtype in bone. *Nature* *507*, 323–328. <https://doi.org/10.1038/nature13145>.
20. Kalucka, J., de Rooij, L.P.M.H., Goveia, J., Rohlenova, K., Dumas, S.J., Meta, E., Concinha, N.V., Taverna, F., Teuwen, L.A., Veys, K., et al. (2020). Single-cell transcriptome atlas of murine endothelial cells. *Cell* *180*, 764–779.e20. <https://doi.org/10.1016/j.cell.2020.01.015>.
21. Muhl, L., Genové, G., Leptidis, S., Liu, J., He, L., Mocci, G., Sun, Y., Gustafsson, S., Buyandelger, B., Chivukula, I.V., et al. (2020). Single-cell analysis uncovers fibroblast heterogeneity and criteria for fibroblast and mural cell identification and discrimination. *Nat. Commun.* *11*, 3953. <https://doi.org/10.1038/s41467-020-17740-1>.
22. Gao, P., Chen, C., Howell, E.D., Li, Y., Tober, J., Uzun, Y., He, B., Gao, L., Zhu, Q., Siekmann, A.F., et al. (2020). Transcriptional regulatory network controlling the ontogeny of hematopoietic stem cells. *Genes Dev.* *34*, 950–964. <https://doi.org/10.1101/gad.338202.120>.
23. Hermiston, M.L., Gupta, V., and Weiss, A. (2010). Chapter 95 - CD45. In *Handbook of Cell Signaling*, Second Edition, R.A. Bradshaw and E.A. Dennis, eds. (Academic Press), pp. 743–748. <https://doi.org/10.1016/B978-0-12-374145-5.00095-4>.
24. Welch, J.J., Watts, J.A., Vakoc, C.R., Yao, Y., Wang, H., Hardison, R.C., Blobel, G.A., Chodosh, L.A., and Weiss, M.J. (2004). Global regulation of erythroid gene expression by transcription factor GATA-1. *Blood* *104*, 3136–3147. <https://doi.org/10.1182/blood-2004-04-1603>.
25. Wolf, F.A., Hamey, F.K., Plass, M., Solana, J., Dahlin, J.S., Göttgens, B., Rajewsky, N., Simon, L., and Theis, F.J. (2019). PAGA: graph abstraction reconciles clustering with trajectory inference through a topology preserving map of single cells. *Genome Biol.* *20*, 59. <https://doi.org/10.1186/s13059-019-1663-x>.
26. Dobnikar, L., Taylor, A.L., Chappell, J., Oldach, P., Harman, J.L., Oerton, E., Dzierzak, E., Bennett, M.R., Spivakov, M., and Jørgensen, H.F. (2018). Disease-relevant transcriptional signatures identified in individual smooth muscle cells from healthy mouse vessels. *Nat. Commun.* *9*, 4567. <https://doi.org/10.1038/s41467-018-06891-x>.
27. Armulik, A., Genové, G., and Betsholtz, C. (2011). Pericytes: developmental, physiological, and pathological perspectives, problems, and promises. *Dev. Cell* *21*, 193–215. <https://doi.org/10.1016/j.devcel.2011.07.001>.
28. Zhang, J., Raper, A., Sugita, N., Hingorani, R., Salio, M., Palmowski, M.J., Cerundolo, V., and Crocker, P.R. (2006). Characterization of Siglec-H as a novel endocytic receptor expressed on murine plasmacytoid dendritic cell precursors. *Blood* *107*, 3600–3608. <https://doi.org/10.1182/blood-2005-09-3842>.
29. Reitz, M., Brunn, M.L., Rodewald, H.R., Feyerabend, T.B., Roers, A., Dudeck, A., Voehringer, D., Jönsson, F., Kühl, A.A., and Breloer, M. (2017). Mucosal mast cells are indispensable for the timely termination of *Strongyloides ratti* infection. *Mucosal Immunol.* *10*, 481–492. <https://doi.org/10.1038/mi.2016.56>.
30. Readinger, J.A., Mueller, K.L., Venegas, A.M., Horai, R., and Schwartzberg, P.L. (2009). Tec kinases regulate T-lymphocyte development and function: new insights into the roles of Itk and Rlk/Tkk. *Immunol. Rev.* *228*, 93–114. <https://doi.org/10.1111/j.1600-065X.2008.00757.x>.
31. Gamage, A.M., Zhu, F., Ahn, M., Foo, R.J.H., Hey, Y.Y., Low, D.H.W., Mendenhall, I.H., Dutertre, C.A., and Wang, L.F. (2020). Immunophenotyping monocytes, macrophages and granulocytes in the Pteropodid bat *Eonycteris spelaea*. *Sci. Rep.* *10*, 309. <https://doi.org/10.1038/s41598-019-57212-1>.
32. Paul, F., Arkin, Y., Giladi, A., Jaitin, D.A., Kenigsberg, E., Keren-Shaul, H., Winter, D., Lara-Astiaso, D., Gury, M., Weiner, A., et al. (2015). Transcriptional heterogeneity and lineage commitment in myeloid progenitors. *Cell* *163*, 1663–1677. <https://doi.org/10.1016/j.cell.2015.11.013>.
33. Yáñez, A., Coetzee, S.G., Olsson, A., Muench, D.E., Berman, B.P., Hazelett, D.J., Salomonis, N., Grimes, H.L., and Goodridge, H.S. (2017). Granulocyte-monocyte progenitors and monocyte-dendritic cell progenitors independently produce functionally distinct monocytes. *Immunity* *47*, 890–902.e4. <https://doi.org/10.1016/j.immuni.2017.10.021>.
34. Zheng, J., Kitajima, K., Sakai, E., Kimura, T., Minegishi, N., Yamamoto, M., and Nakano, T. (2006). Differential effects of GATA-1 on proliferation and differentiation of erythroid lineage cells. *Blood* *107*, 520–527. <https://doi.org/10.1182/blood-2005-04-1385>.
35. Summers, K.M., Bush, S.J., and Hume, D.A. (2020). Network analysis of transcriptomic diversity amongst resident tissue macrophages and dendritic cells in the mouse mononuclear phagocyte system. *PLoS Biol.* *18*, e3000859. <https://doi.org/10.1371/journal.pbio.3000859>.
36. Grieshaber-Bouyer, R., Radtke, F.A., Cunin, P., Stifano, G., Levescot, A., Vijaykumar, B., Nelson-Maney, N., Blaustein, R.B., Monach, P.A., and Nigrovic, P.A.; ImmGen Consortium (2021). The neutrotime transcriptional signature defines a single continuum of neutrophils across biological compartments. *Nat. Commun.* *12*, 2856. <https://doi.org/10.1038/s41467-021-22973-9>.
37. Nutt, S.L., and Kee, B.L. (2007). The transcriptional regulation of B cell lineage commitment. *Immunity* *26*, 715–725. <https://doi.org/10.1016/j.immuni.2007.05.010>.
38. Cochain, C., Vafadarnejad, E., Arampatzis, P., Pelisek, J., Winkels, H., Ley, K., Wolf, D., Saliba, A.E., and Zernecke, A. (2018). Single-cell RNA-seq reveals the transcriptional landscape and heterogeneity of aortic macrophages in murine atherosclerosis. *Circ. Res.* *122*, 1661–1674. <https://doi.org/10.1161/circresaha.117.312509>.
39. Takeshita, S., Kaji, K., and Kudo, A. (2000). Identification and characterization of the new osteoclast progenitor with macrophage phenotypes being able to

- differentiate into mature osteoclasts. *J. Bone Miner. Res.* 15, 1477–1488. <https://doi.org/10.1359/jbmr.2000.15.8.1477>.
40. Teo, B.H.D., Bobryshev, Y.V., Teh, B.K., Wong, S.H., and Lu, J. (2012). Complement C1q production by osteoclasts and its regulation of osteoclast development. *Biochem. J.* 447, 229–237. <https://doi.org/10.1042/bj20120888>.
  41. Tsukasaki, M., Huynh, N.C.-N., Okamoto, K., Muro, R., Terashima, A., Kurikawa, Y., Komatsu, N., Pluemsakunthai, W., Nitta, T., Abe, T., et al. (2020). Stepwise cell fate decision pathways during osteoclastogenesis at single-cell resolution. *Nat. Metab.* 2, 1382–1390. <https://doi.org/10.1038/s42255-020-00318-y>.
  42. Zhang, Q., Riddle, R.C., and Clemens, T.L. (2015). Bone and the regulation of global energy balance. *J. Intern. Med.* 277, 681–689. <https://doi.org/10.1111/joim.12348>.
  43. Walzer, S.M., Cetin, E., Grübl-Barabas, R., Sulzbacher, I., Rueger, B., Girsch, W., Toegel, S., Windhager, R., and Fischer, M.B. (2014). Vascularization of primary and secondary ossification centres in the human growth plate. *BMC Dev. Biol.* 14, 36. <https://doi.org/10.1186/s12861-014-0036-7>.
  44. Nicoletti, C., Wei, X., Etxaniz, U., Proietti, D., Madaro, L., and Puri, P.L. (2020). scRNA-seq-based analysis of skeletal muscle response to denervation reveals selective activation of muscle-resident glial cells and fibroblasts. Preprint at bioRxiv. <https://doi.org/10.1101/2020.12.29.424762>.
  45. Qiu, X., Mao, Q., Tang, Y., Wang, L., Chawla, R., Pliener, H.A., and Trapnell, C. (2017). Reversed graph embedding resolves complex single-cell trajectories. *Nat. Methods* 14, 979–982. <https://doi.org/10.1038/nmeth.4402>.
  46. Cao, J., Spielmann, M., Qiu, X., Huang, X., Ibrahim, D.M., Hill, A.J., Zhang, F., Mundlos, S., Christiansen, L., Steemers, F.J., et al. (2019). The single-cell transcriptional landscape of mammalian organogenesis. *Nature* 566, 496–502. <https://doi.org/10.1038/s41586-019-0969-x>.
  47. Mori-Akiyama, Y., Akiyama, H., Rowitch, D.H., and de Crombrugge, B. (2003). Sox9 is required for determination of the chondrogenic cell lineage in the cranial neural crest. *Proc. Natl. Acad. Sci. USA* 100, 9360–9365. <https://doi.org/10.1073/pnas.1631288100>.
  48. Ionescu, A., Kozhemyakina, E., Nicolae, C., Kaestner, K.H., Olsen, B.R., and Lassar, A.B. (2012). FoxA family members are crucial regulators of the hypertrophic chondrocyte differentiation program. *Dev. Cell* 22, 927–939. <https://doi.org/10.1016/j.devcel.2012.03.011>.
  49. Yoshida, M., Hata, K., Takashima, R., Ono, K., Nakamura, E., Takahata, Y., Murakami, T., Iseki, S., Takano-Yamamoto, T., Nishimura, R., and Yoneda, T. (2015). The transcription factor Foxc1 is necessary for Ihh-Gli2-regulated endochondral ossification. *Nat. Commun.* 6, 6653. <https://doi.org/10.1038/ncomms7653>.
  50. Jones, F.S., Kioussi, C., Copertino, D.W., Kallunki, P., Holst, B.D., and Edelman, G.M. (1997). Barx2, a new homeobox gene of the Bar class, is expressed in neural and craniofacial structures during development. *Proc. Natl. Acad. Sci. USA* 94, 2632–2637. <https://doi.org/10.1073/pnas.94.6.2632>.
  51. Dreher, S.I., Fischer, J., Walker, T., Diederichs, S., and Richter, W. (2020). Significance of MEF2C and RUNX3 regulation for endochondral differentiation of human mesenchymal progenitor cells. *Front. Cell Dev. Biol.* 8, 81. <https://doi.org/10.3389/fcell.2020.00081>.
  52. Vignali, R., and Marracci, S. (2020). HMGA genes and proteins in development and evolution. *Int. J. Mol. Sci.* 21, 654. <https://doi.org/10.3390/ijms21020654>.
  53. Bye-A-Jee, H., Pugazhendhi, D., Woodhouse, S., Brien, P., Watson, R., Turner, M., and Pell, J. (2018). The RNA-binding proteins Zfp361 and Zfp362 act redundantly in myogenesis. *Skeletal Muscle* 8, 37. <https://doi.org/10.1186/s13395-018-0183-9>.
  54. Mathew, S.J., Hansen, J.M., Merrell, A.J., Murphy, M.M., Lawson, J.A., Hutcheson, D.A., Hansen, M.S., Angus-Hill, M., and Kardon, G. (2011). Connective tissue fibroblasts and Tcf4 regulate myogenesis. *Development* 138, 371–384. <https://doi.org/10.1242/dev.057463>.
  55. Chen, S.X., Cherry, A., Tari, P.K., Podgorski, K., Kwong, Y.K.K., and Haas, K. (2012). The transcription factor MEF2 directs developmental visually driven functional and structural metaplasticity. *Cell* 151, 41–55. <https://doi.org/10.1016/j.cell.2012.08.028>.
  56. Ma, B., Zhong, L., van Blitterswijk, C.A., Post, J.N., and Karperien, M. (2013). T cell factor 4 is a pro-catabolic and apoptotic factor in human articular chondrocytes by potentiating nuclear factor κB signaling. *J. Biol. Chem.* 288, 17552–17558. <https://doi.org/10.1074/jbc.M113.453985>.
  57. Son, Y.O., Kim, H.E., Choi, W.S., Chun, C.H., and Chun, J.S. (2019). RNA-binding protein ZFP36L1 regulates osteoarthritis by modulating members of the heat shock protein 70 family. *Nat. Commun.* 10, 77. <https://doi.org/10.1038/s41467-018-08035-7>.
  58. Mi, H., Muruganujan, A., Casagrande, J.T., and Thomas, P.D. (2013). Large-scale gene function analysis with the PANTHER classification system. *Nat. Protoc.* 8, 1551–1566. <https://doi.org/10.1038/nprot.2013.092>.
  59. Gansner, J.M., and Gitlin, J.D. (2008). Essential role for the alpha 1 chain of type VIII collagen in zebrafish notochord formation. *Dev. Dynam.* 237, 3715–3726. <https://doi.org/10.1002/dvdy.21779>.
  60. Zhang, C.-H., Gao, Y., Jadhav, U., Hung, H.-H., Holton, K.M., Grodzinsky, A.J., Shivdasani, R.A., and Lassar, A.B. (2021). Creb5 establishes the competence for Prg4 expression in articular cartilage. *Commun. Biol.* 4, 332. <https://doi.org/10.1038/s42003-021-01857-0>.
  61. Hissnauer, T.N., Baranowsky, A., Pestka, J.M., Streichert, T., Wiegandt, K., Goepfert, C., Beil, F.T., Albers, J., Schulze, J., Ueblacker, P., et al. (2010). Identification of molecular markers for articular cartilage. *Osteoarthritis Cartilage* 18, 1630–1638. <https://doi.org/10.1016/j.joca.2010.10.002>.
  62. Kania, K., Colella, F., Riemen, A.H.K., Wang, H., Howard, K.A., Aigner, T., Dell’Accio, F., Capellini, T.D., Roelofs, A.J., and De Bari, C. (2020). Regulation of Gdf5 expression in joint remodelling, repair and osteoarthritis. *Sci. Rep.* 10, 157. <https://doi.org/10.1038/s41598-019-57011-8>.
  63. Wu, L., Blugermann, C., Kyupelyan, L., Latour, B., Gonzalez, S., Shah, S., Galic, Z., Ge, S., Zhu, Y., Petrigliano, F.A., et al. (2013). Human developmental chondrogenesis as a basis for engineering chondrocytes from pluripotent stem cells. *Stem Cell Rep.* 1, 575–589. <https://doi.org/10.1016/j.stemcr.2013.10.012>.
  64. Lorenzo, P., Bayliss, M.T., and Heinegård, D. (1998). A novel cartilage protein (CILP) present in the mid-zone of human articular cartilage increases with age. *J. Biol. Chem.* 273, 23463–23468. <https://doi.org/10.1074/jbc.273.36.23463>.
  65. Bian, Q., Cheng, Y.H., Wilson, J.P., Su, E.Y., Kim, D.W., Wang, H., Yoo, S., Blackshaw, S., and Cahan, P. (2020). A single cell transcriptional atlas of early synovial joint development. *Development* 147. <https://doi.org/10.1242/dev.185777>.
  66. Jeon, S., and Seong, R.H. (2016). Anteroposterior limb skeletal patterning requires the bifunctional action of SWI/SNF chromatin remodeling complex in hedgehog pathway. *PLoS Genet.* 12, e1005915. <https://doi.org/10.1371/journal.pgen.1005915>.
  67. Imamura, K., Maeda, S., Kawamura, I., Matsuyama, K., Shinohara, N., Yahiro, Y., Nagano, S., Setoguchi, T., Yokouchi, M., Ishidou, Y., and Komiya, S. (2014). Human immunodeficiency virus type 1 enhancer-binding protein 3 is essential for the expression of asparagine-linked glycosylation 2 in the regulation of osteoblast and chondrocyte differentiation. *J. Biol. Chem.* 289, 9865–9879. <https://doi.org/10.1074/jbc.M113.520585>.
  68. Schmid, R., Meyer, K., Spang, R., Schittek, B., and Bosserhoff, A.K. (2013). YBX1 is a modulator of MIA/CD-RAP-dependent chondrogenesis. *PLoS One* 8, e82166. <https://doi.org/10.1371/journal.pone.0082166>.
  69. Gu, J., Lu, Y., Li, F., Qiao, L., Wang, Q., Li, N., Borgia, J.A., Deng, Y., Lei, G., and Zheng, Q. (2014). Identification and characterization of the novel Col10a1 regulatory mechanism during chondrocyte hypertrophic differentiation. *Cell Death Dis.* 5, e1469. <https://doi.org/10.1038/cddis.2014.444>.

70. Cesario, J.M., Almaidhan, A.A., and Jeong, J. (2016). Expression of forkhead box transcription factor genes *Foxp1* and *Foxp2* during jaw development. *Gene Expr. Patterns* 20, 111–119. <https://doi.org/10.1016/j.gep.2016.03.001>.
71. L ejard, V., Brideau, G., Blais, F., Salingcamboriboon, R., Wagner, G., Roehrl, M.H.A., Noda, M., Duprez, D., Houillier, P., and Rossert, J. (2007). Scleraxis and NFATc regulate the expression of the pro- $\alpha$ 1(I) collagen gene in tendon fibroblasts. *J. Biol. Chem.* 282, 17665–17675. <https://doi.org/10.1074/jbc.M610113200>.
72. Roelofs, A.J., Kania, K., Rafipay, A.J., Sambale, M., Kuwahara, S.T., Collins, F.L., Smeeton, J., Serowoky, M.A., Rowley, L., Wang, H., et al. (2020). Identification of the skeletal progenitor cells forming osteophytes in osteoarthritis. *Ann. Rheum. Dis.* 79, 1625–1634. <https://doi.org/10.1136/annrheumdis-2020-218350>.
73. Farahani, R.M., and Xaymardan, M. (2015). Platelet-derived growth factor receptor alpha as a marker of mesenchymal stem cells in development and stem cell biology. *Stem Cell. Int.* 2015, 362753. <https://doi.org/10.1155/2015/362753>.
74. Ataliotis, P. (2000). Platelet-derived growth factor A modulates limb chondrogenesis both in vivo and in vitro. *Mech. Dev.* 94, 13–24. [https://doi.org/10.1016/s0925-4773\(00\)00321-x](https://doi.org/10.1016/s0925-4773(00)00321-x).
75. Matsumura, T., Saito, Y., Suzuki, T., Teramoto, A., Ozasa, Y., Yamashita, T., Fujimiya, M., and Saito-Chikenji, T. (2019). Phosphorylated platelet-derived growth factor receptor-positive cells with anti-apoptotic properties accumulate in the synovium of patients with rheumatoid arthritis. *Front. Immunol.* 10, 241. <https://doi.org/10.3389/fimmu.2019.00241>.
76. Harvey, T., Flamenco, S., and Fan, C.M. (2019). A *Tppp3(+)*/*Pdgfra(+)* tendon stem cell population contributes to regeneration and reveals a shared role for PDGF signalling in regeneration and fibrosis. *Nat. Cell Biol.* 21, 1490–1503. <https://doi.org/10.1038/s41556-019-0417-z>.
77. Yang, J., Andre, P., Ye, L., and Yang, Y.Z. (2015). The Hedgehog signalling pathway in bone formation. *Int. J. Oral Sci.* 7, 73–79. <https://doi.org/10.1038/ijos.2015.14>.
78. Imuta, Y., Nishioka, N., Kiyonari, H., and Sasaki, H. (2009). Short limbs, cleft palate, and delayed formation of flat proliferative chondrocytes in mice with targeted disruption of a putative protein kinase gene, *Pkdcc* (AW548124). *Dev. Dynam.* 238, 210–222. <https://doi.org/10.1002/dvdy.21822>.
79. Zheng, C., Lin, X., Xu, X., Wang, C., Zhou, J., Gao, B., Fan, J., Lu, W., Hu, Y., Jie, Q., et al. (2019). Suppressing UPR-dependent overactivation of FGFR3 signaling ameliorates SLC26A2-deficient chondrodysplasias. *EBioMedicine* 40, 695–709. <https://doi.org/10.1016/j.ebiom.2019.01.010>.
80. Andrade, A.C., Nilsson, O., Barnes, K.M., and Baron, J. (2007). Wnt gene expression in the post-natal growth plate: regulation with chondrocyte differentiation. *Bone* 40, 1361–1369. <https://doi.org/10.1016/j.bone.2007.01.005>.
81. Ishikawa, M., and Yamada, Y. (2017). The role of pannexin 3 in bone biology. *J. Dent. Res.* 96, 372–379. <https://doi.org/10.1177/0022034516678203>.
82. Li, J., Manickam, G., Ray, S., Oh, C.D., Yasuda, H., Moffatt, P., and Murshed, M. (2016). *Smpd3* expression in both chondrocytes and osteoblasts is required for normal endochondral bone development. *Mol. Cell Biol.* 36, 2282–2299. <https://doi.org/10.1128/mcb.01077-15>.
83. Mirzamohammadi, F., Papaioannou, G., Inloes, J.B., Rankin, E.B., Xie, H., Schipani, E., Orkin, S.H., and Kobayashi, T. (2016). Polycomb repressive complex 2 regulates skeletal growth by suppressing Wnt and TGF- $\beta$  signalling. *Nat. Commun.* 7, 12047. <https://doi.org/10.1038/ncomms12047>.
84. Vortkamp, A., Lee, K., Lanske, B., Segre, G.V., Kronenberg, H.M., and Tabin, C.J. (1996). Regulation of rate of cartilage differentiation by Indian hedgehog and PTH-related protein. *Science* 273, 613–622. <https://doi.org/10.1126/science.273.5275.613>.
85. Lanske, B., Karaplis, A.C., Lee, K., Luz, A., Vortkamp, A., Pirro, A., Karperien, M., Defize, L.H., Ho, C., Mulligan, R.C., et al. (1996). PTH/PTHrP receptor in early development and Indian hedgehog-regulated bone growth. *Science* 273, 663–666. <https://doi.org/10.1126/science.273.5275.663>.
86. Prein, C., Warmbold, N., Farkas, Z., Schieker, M., Aszodi, A., and Clausen-Schaumann, H. (2016). Structural and mechanical properties of the proliferative zone of the developing murine growth plate cartilage assessed by atomic force microscopy. *Matrix Biol.* 50, 1–15. <https://doi.org/10.1016/j.matbio.2015.10.001>.
87. Lui, J.C.K., Andrade, A.C., Forcinito, P., Hegde, A., Chen, W., Baron, J., and Nilsson, O. (2010). Spatial and temporal regulation of gene expression in the mammalian growth plate. *Bone* 46, 1380–1390. <https://doi.org/10.1016/j.bone.2010.01.373>.
88. Gao, M.M., Su, Q.N., Liang, T.Z., Ma, J.X., Liang, T.Z., Stoddart, M.J., Richards, R.G., Zhou, Z.Y., and Zou, N.X. (2018). Transcriptional activation of ENPP1 by osterix in osteoblasts and osteocytes. *Eur. Cell. Mater.* 36, 1–14. <https://doi.org/10.22203/eCM.v036a01>.
89. Bahamonde, M.E., and Lyons, K.M. (2001). BMP3: to be or not to be a BMP. *J. Bone Joint Surg. Am.* 83-A, S56–S62.
90. Witte, F., Dokas, J., Neuendorf, F., Mndlos, S., and Stricker, S. (2009). Comprehensive expression analysis of all Wnt genes and their major secreted antagonists during mouse limb development and cartilage differentiation. *Gene Expr. Patterns* 9, 215–223. <https://doi.org/10.1016/j.gep.2008.12.009>.
91. Caron, M.M.J., Emans, P.J., Cremers, A., Surtel, D.A.M., Coolsen, M.M.E., van Rhijn, L.W., and Welting, T.J.M. (2013). Hypertrophic differentiation during chondrogenic differentiation of progenitor cells is stimulated by BMP-2 but suppressed by BMP-7. *Osteoarthritis Cartilage* 21, 604–613. <https://doi.org/10.1016/j.joca.2013.01.009>.
92. Tu, X., Joeng, K.S., Nakayama, K.I., Nakayama, K., Rajagopal, J., Carroll, T.J., McMahon, A.P., and Long, F. (2007). Noncanonical Wnt signaling through G protein-linked PKC $\delta$  activation promotes bone formation. *Dev. Cell* 12, 113–127. <https://doi.org/10.1016/j.devcel.2006.11.003>.
93. Yoshida, C.A., Yamamoto, H., Fujita, T., Furuichi, T., Ito, K., Inoue, K.I., Yamana, K., Zanma, A., Takada, K., Ito, Y., and Komori, T. (2004). Runx2 and Runx3 are essential for chondrocyte maturation, and Runx2 regulates limb growth through induction of Indian hedgehog. *Genes Dev.* 18, 952–963. <https://doi.org/10.1101/gad.1174704>.
94. Tan, Z., Kong, M., Wen, S., Tsang, K.Y., Niu, B., Hartmann, C., Chan, D., Hui, C.C., and Cheah, K.S.E. (2020). IRX3 and IRX5 inhibit adipogenic differentiation of hypertrophic chondrocytes and promote osteogenesis. *J. Bone Miner. Res.* 35, 2444–2457. <https://doi.org/10.1002/jbmr.4132>.
95. Arnold, M.A., Kim, Y., Czubyrt, M.P., Phan, D., McAnally, J., Qi, X., Shelton, J.M., Richardson, J.A., Bassel-Duby, R., and Olson, E.N. (2007). MEF2C transcription factor controls chondrocyte hypertrophy and bone development. *Dev. Cell* 12, 377–389. <https://doi.org/10.1016/j.devcel.2007.02.004>.
96. Gerber, H.P., Vu, T.H., Ryan, A.M., Kowalski, J., Werb, Z., and Ferrara, N. (1999). VEGF couples hypertrophic cartilage remodeling, ossification and angiogenesis during endochondral bone formation. *Nat. Med.* 5, 623–628. <https://doi.org/10.1038/9467>.
97. Jin, S., Guerrero-Juarez, C.F., Zhang, L., Chang, I., Ramos, R., Kuan, C.-H., Myung, P., Plikus, M.V., and Nie, Q. (2021). Inference and analysis of cell-cell communication using CellChat. *Nat. Commun.* 12, 1088. <https://doi.org/10.1038/s41467-021-21246-9>.
98. Decker, R.S. (2017). Articular cartilage and joint development from embryogenesis to adulthood. *Semin. Cell Dev. Biol.* 62, 50–56. <https://doi.org/10.1016/j.semcdb.2016.10.005>.
99. Salzmann, G.M., Niemeyer, P., Hochrein, A., Stoddart, M.J., and Angele, P. (2018). Articular cartilage repair of the knee in children and adolescents. *Orthop. J. Sports Med.* 6, 2325967118760190. <https://doi.org/10.1177/2325967118760190>.
100. Jenner, F., Ijpma, A., Cleary, M., Heijnsman, D., Narcisi, R., van der Spek, P.J., Kremer, A., van Weeren, R., Brama, P., van Osch, G.J.,

- and van Osch, G.J.V.M. (2014). Differential gene expression of the intermediate and outer interzone layers of developing articular cartilage in murine embryos. *Stem Cell. Dev.* 23, 1883–1898. <https://doi.org/10.1089/scd.2013.0235>.
101. Kozhemyakina, E., Zhang, M., Ionescu, A., Ayturk, U.M., Ono, N., Kobayashi, A., Kronenberg, H., Warman, M.L., and Lassar, A.B. (2015). Identification of a Prg4-expressing articular cartilage progenitor cell population in mice. *Arthritis Rheumatol.* 67, 1261–1273. <https://doi.org/10.1002/art.39030>.
102. Koyama, E., Shibukawa, Y., Nagayama, M., Sugito, H., Young, B., Yuasa, T., Okabe, T., Ochiai, T., Kamiya, N., Rountree, R.B., et al. (2008). A distinct cohort of progenitor cells participates in synovial joint and articular cartilage formation during mouse limb skeletogenesis. *Dev. Biol.* 316, 62–73. <https://doi.org/10.1016/j.ydbio.2008.01.012>.
103. Decker, R.S., Um, H.B., Dymont, N.A., Cottingham, N., Usami, Y., Enomoto-Iwamoto, M., Kronenberg, M.S., Maye, P., Rowe, D.W., Koyama, E., and Pacifici, M. (2017). Cell origin, volume and arrangement are drivers of articular cartilage formation, morphogenesis and response to injury in mouse limbs. *Dev. Biol.* 426, 56–68. <https://doi.org/10.1016/j.ydbio.2017.04.006>.
104. Rolauffs, B., Williams, J.M., Aurich, M., Grodzinsky, A.J., Kuettner, K.E., and Cole, A.A. (2010). Proliferative remodeling of the spatial organization of human superficial chondrocytes distant from focal early osteoarthritis. *Arthritis Rheum.* 62, 489–498. <https://doi.org/10.1002/art.27217>.
105. Long, H., Zeng, X., Liu, Q., Wang, H., Vos, T., Hou, Y., Lin, C., Qiu, Y., Wang, K., Xing, D., et al. (2020). Burden of osteoarthritis in China, 1990–2017: findings from the global burden of disease study 2017. *Lancet Rheumatol.* 2, e164–e172. [https://doi.org/10.1016/S2665-9913\(19\)30145-6](https://doi.org/10.1016/S2665-9913(19)30145-6).
106. Hunter, D.J., and Bierma-Zeinstra, S. (2019). Osteoarthritis. *Lancet* 393, 1745–1759. [https://doi.org/10.1016/S0140-6736\(19\)30417-9](https://doi.org/10.1016/S0140-6736(19)30417-9).
107. Fitzgerald, J., Rich, C., Burkhardt, D., Allen, J., Herzka, A.S., and Little, C.B. (2008). Evidence for articular cartilage regeneration in MRL/MpJ mice. *Osteoarthritis Cartilage* 16, 1319–1326. <https://doi.org/10.1016/j.joca.2008.03.014>.
108. Fitzgerald, J. (2017). Enhanced cartilage repair in ‘healer’ mice-New leads in the search for better clinical options for cartilage repair. *Semin. Cell Dev. Biol.* 62, 78–85. <https://doi.org/10.1016/j.semcdb.2016.04.018>.
109. Rai, M.F., Schmidt, E.J., McAlinden, A., Cheverud, J.M., and Sandell, L.J. (2013). Molecular insight into the association between cartilage regeneration and ear wound healing in genetic mouse models: targeting new genes in regeneration. *G3 (Bethesda)* 3, 1881–1891. <https://doi.org/10.1534/g3.113.007302>.
110. Krajewska-Włodarczyk, M., Owczarczyk-Saczonek, A., Placek, W., Osowski, A., and Wojtkiewicz, J. (2018). Articular cartilage aging-potential regenerative capacities of cell manipulation and stem cell therapy. *Int. J. Mol. Sci.* 19, 623. <https://doi.org/10.3390/ijms19020623>.
111. Civin, C.I., Strauss, L.C., Brovall, C., Fackler, M.J., Schwartz, J.F., and Shaper, J.H. (1984). Antigenic analysis of hematopoiesis. III. A hematopoietic progenitor cell surface antigen defined by a monoclonal antibody raised against KG-1a cells. *J. Immunol.* 133, 157–165.
112. Joe, A.W.B., Yi, L., Natarajan, A., Le Grand, F., So, L., Wang, J., Rudnicki, M.A., and Rossi, F.M.V. (2010). Muscle injury activates resident fibro/adipogenic progenitors that facilitate myogenesis. *Nat. Cell Biol.* 12, 153–163. <https://doi.org/10.1038/ncb2015>.
113. García-Prat, L., Perdiguero, E., Alonso-Martin, S., Dell’Orso, S., Ravichandran, S., Brooks, S.R., Juan, A.H., Campanario, S., Jiang, K., Hong, X., et al. (2020). FoxO maintains a genuine muscle stem-cell quiescent state until geriatric age. *Nat. Cell Biol.* 22, 1307–1318. <https://doi.org/10.1038/s41556-020-00593-7>.
114. Sidney, L.E., Branch, M.J., Dunphy, S.E., Dua, H.S., and Hopkinson, A. (2014). Concise review: evidence for CD34 as a common marker for diverse progenitors. *Stem Cell.* 32, 1380–1389. <https://doi.org/10.1002/stem.1661>.
115. Bland, Y.S., and Ashhurst, D.E. (1997). Fetal and postnatal development of the patella, patellar tendon and suprapatella in the rabbit; changes in the distribution of the fibrillar collagens. *J. Anat.* 190, 327–342. <https://doi.org/10.1046/j.1469-7580.1997.19030327.x>.
116. Galatz, L., Rothermich, S., Vanderploeg, K., Petersen, B., Sandell, L., and Thomopoulos, S. (2007). Development of the supraspinatus tendon-to-bone insertion: localized expression of extracellular matrix and growth factor genes. *J. Orthop. Res.* 25, 1621–1628. <https://doi.org/10.1002/jor.20441>.
117. Woo, S.L., and Buckwalter, J.A. (1988). Injury and repair of the musculoskeletal soft tissues. Savannah, Georgia, June 18–20, 1987. *J. Orthop. Res.* 6, 907–931. <https://doi.org/10.1002/jor.1100060615>.
118. Thomopoulos, S., Genin, G.M., and Galatz, L.M. (2010). The development and morphogenesis of the tendon-to-bone insertion - what development can teach us about healing. *J. Musculoskelet. Neuronal Interact.* 10, 35–45.
119. Apostolakis, J., Durant, T.J., Dwyer, C.R., Russell, R.P., Weinreb, J.H., Alaei, F., Beitzel, K., McCarthy, M.B., Cote, M.P., and Mazzocca, A.D. (2014). The enthesis: a review of the tendon-to-bone insertion. *Muscles Ligaments Tendons J.* 4, 333–342.
120. Kronenberg, H.M. (2003). Developmental regulation of the growth plate. *Nature* 423, 332–336. <https://doi.org/10.1038/nature01657>.
121. Chagin, A.S., and Newton, P.T. (2020). Postnatal skeletal growth is driven by the epiphyseal stem cell niche: potential implications to pediatrics. *Pediatr. Res.* 87, 986–990. <https://doi.org/10.1038/s41390-019-0722-z>.
122. Xie, M., Gol’din, P., Herdina, A.N., Estefa, J., Medvedeva, E.V., Li, L., Newton, P.T., Kotova, S., Shavkuta, B., Saxena, A., et al. (2020). Secondary ossification center induces and protects growth plate structure. *Elife* 9, e55212. <https://doi.org/10.7554/eLife.55212>.
123. Castañeda, S., Largo, R., Calvo, E., Rodríguez-Salvanés, F., Marcos, M.E., Díaz-Curiel, M., and Herrero-Beaumont, G. (2006). Bone mineral measurements of subchondral and trabecular bone in healthy and osteoporotic rabbits. *Skeletal Radiol.* 35, 34–41. <https://doi.org/10.1007/s00256-005-0022-z>.
124. Fernández-Iglesias, Á., Fuente, R., Gil-Peña, H., Alonso-Durán, L., Santos, F., and López, J.M. (2021). The Formation of the epiphyseal bone plate occurs via combined endochondral and intramembranous-like ossification. *Int. J. Mol. Sci.* 22, 900. <https://doi.org/10.3390/ijms22020900>.
125. Ni, R., Guo, X.E., Yan, C., and Wen, C. (2022). Hemodynamic stress shapes subchondral bone in osteoarthritis: an emerging hypothesis. *J. Orthop. Translat.* 32, 85–90. <https://doi.org/10.1016/j.jot.2021.11.007>.
126. Chen, L., Zheng, J.J.Y., Li, G., Yuan, J., Ebert, J.R., Li, H., Papadimitriou, J., Wang, Q., Wood, D., Jones, C.W., and Zheng, M. (2020). Pathogenesis and clinical management of obesity-related knee osteoarthritis: impact of mechanical loading. *J. Orthop. Translat.* 24, 66–75. <https://doi.org/10.1016/j.jot.2020.05.001>.
127. Kalvaityte, U., Matta, C., Bernotiene, E., Pushparaj, P.N., Kiapour, A.M., and Mobasher, A. (2022). Exploring the translational potential of clusterin as a biomarker of early osteoarthritis. *J. Orthop. Translat.* 32, 77–84. <https://doi.org/10.1016/j.jot.2021.10.001>.
128. Mapp, P.I., and Walsh, D.A. (2012). Mechanisms and targets of angiogenesis and nerve growth in osteoarthritis. *Nat. Rev. Rheumatol.* 8, 390–398. <https://doi.org/10.1038/nrrheum.2012.80>.
129. van der Kraan, P.M., and van den Berg, W.B. (2012). Chondrocyte hypertrophy and osteoarthritis: role in initiation and progression of cartilage degeneration? *Osteoarthritis Cartilage* 20, 223–232. <https://doi.org/10.1016/j.joca.2011.12.003>.
130. Bonnet, C.S., and Walsh, D.A. (2005). Osteoarthritis, angiogenesis and inflammation. *Rheumatology* 44, 7–16. <https://doi.org/10.1093/rheumatology/keh344>.
131. Chen, D., Shen, J., Zhao, W., Wang, T., Han, L., Hamilton, J.L., and Im, H.J. (2017). Osteoarthritis: toward a comprehensive understanding of pathological mechanism.

- Bone Res. 5, 16044. <https://doi.org/10.1038/boneres.2016.44>.
132. Pitsillides, A.A., and Beier, F. (2011). Cartilage biology in osteoarthritis—lessons from developmental biology. *Nat. Rev. Rheumatol.* 7, 654–663. <https://doi.org/10.1038/nrrheum.2011.129>.
133. Salhotra, A., Shah, H.N., Levi, B., and Longaker, M.T. (2020). Mechanisms of bone development and repair. *Nat. Rev. Mol. Cell Biol.* 21, 696–711. <https://doi.org/10.1038/s41580-020-00279-w>.
134. Tong, W., Zeng, Y., Chow, D.H.K., Yeung, W., Xu, J., Deng, Y., Chen, S., Zhao, H., Zhang, X., Ho, K.K., et al. (2019). Wnt16 attenuates osteoarthritis progression through a PCP/JNK-mTORC1-PTHrP cascade. *Ann. Rheum. Dis.* 78, 551–561. <https://doi.org/10.1136/annrheumdis-2018-214200>.
135. Wolf, F.A., Angerer, P., and Theis, F.J. (2018). SCANPY: large-scale single-cell gene expression data analysis. *Genome Biol.* 19, 15. <https://doi.org/10.1186/s13059-017-1382-0>.
136. Yu, G., Wang, L.-G., Han, Y., and He, Q.-Y. (2012). clusterProfiler: an R Package for comparing biological themes among gene clusters. *OMICS* 16, 284–287. <https://doi.org/10.1089/omi.2011.0118>.
137. Gao, M., Guo, P., Liu, X., Zhang, P., He, Z., Wen, L., Liu, S., Zhou, Z., and Zhu, W. (2022). Systematic study of single-cell isolation from musculoskeletal tissues for single-cell sequencing. *BMC Mol. Cell Biol.* 23, 32. <https://doi.org/10.1186/s12860-022-00429-2>.
138. Hu, H., Miao, Y.R., Jia, L.H., Yu, Q.Y., Zhang, Q., and Guo, A.Y. (2019). AnimalTFDB 3.0: a comprehensive resource for annotation and prediction of animal transcription factors. *Nucleic Acids Res.* 47, D33–d38. <https://doi.org/10.1093/nar/gky822>.
139. Bausch-Fluck, D., Hofmann, A., Bock, T., Frei, A.P., Cerciello, F., Jacobs, A., Moest, H., Omasits, U., Gundry, R.L., Yoon, C., et al. (2015). A mass spectrometric-derived cell surface protein atlas. *PLoS One* 10, e0121314. <https://doi.org/10.1371/journal.pone.0121314>.
140. Kusumbe, A.P., Ramasamy, S.K., Starsichova, A., and Adams, R.H. (2015). Sample preparation for high-resolution 3D confocal imaging of mouse skeletal tissue. *Nat. Protoc.* 10, 1904–1914. <https://doi.org/10.1038/nprot.2015.125>.

## STAR★METHODS

## KEY RESOURCES TABLE

REAGENT or RESOURCE	SOURCE	IDENTIFIER
<b>Antibodies</b>		
Anti-CD34 antibody	Abcam	Cat# ab8158; RRID: AB_306316
CD34 Recombinant Rabbit Monoclonal Antibody	Invitrogen	Cat# MA5-29674; RRID: AB_2785500
Ly6e antibody	Biorbyt	Cat# orb20596; RRID: AB_10751664
Anti-Sca1 antibody	Abcam	Cat# ab51317; RRID: AB_1640946
Tnni2 antibody	ABclonal	Cat# A4740; RRID: AB_2863337
Osteopontin antibody	Affinity Biosciences	Cat# AF0227; RRID: AB_2833402
Anti-Collagen X antibody	Abcam	Cat# ab58632; RRID: AB_879742
Anti-Cd31 antibody	Abcam	Cat# ab222783; RRID: AB_2905525
Endomucin antibody	Santa Cruz Biotechnology	Cat# sc-65495; RRID: AB_2100037
Cy <sup>TM</sup> 3 AffiniPure F(ab') <sub>2</sub> Fragment Donkey Anti-Goat IgG (H + L)	Jackson ImmunoResearch	Cat# 705-166-147; RRID: AB_2340413
Alexa Fluor® 594 AffiniPure F(ab') <sub>2</sub> Fragment Donkey Anti-Rabbit IgG (H + L)	Jackson ImmunoResearch	Cat# 711-586-152; RRID: AB_2340622
Donkey polyclonal Secondary Antibody to Rat IgG - H&L (Alexa Fluor® 647)	Abcam	Cat# ab150155; RRID: AB_2813835
Donkey anti-Rabbit IgG (H + L) Highly Cross-Adsorbed Secondary Antibody, Alexa Fluor Plus 555	Invitrogen	Cat# A32794; RRID: AB_2762834
<b>Critical commercial assays</b>		
Chromium Single Cell 3' Reagent Kits v3	10× Genomics	PN-1000075, PN-1000073, PN-120262
Chromium Single Cell Chip B	10× Genomics	2000060
<b>Deposited data</b>		
ScRNA-seq dataset for murine postnatal limbs	This article	BioProject: PRJNA792884
<b>Experimental models: Organisms/strains</b>		
C57BL/6J mice	SPF (Beijing) biotechnology co., LTD	YC0087
<b>Software and algorithms</b>		
Scanpy package (v1.8.2)	Wolf et al. <sup>135</sup>	<a href="https://github.com/scverse/scanpy">https://github.com/scverse/scanpy</a>
R package Monocle 2 (v2.8.0)	Qiu et al. <sup>45</sup>	<a href="https://github.com/Scylardor/Monocle2">https://github.com/Scylardor/Monocle2</a>
ClusterProfiler in R package (v3.10.0)	Yu et al. <sup>136</sup>	<a href="http://bioconductor.org/packages/release/bioc/html/clusterProfiler.html">http://bioconductor.org/packages/release/bioc/html/clusterProfiler.html</a>
CellChat R package (v1.1.0)	Jin et al. <sup>97</sup>	<a href="https://github.com/sqjin/CellChat">https://github.com/sqjin/CellChat</a>

## RESOURCE AVAILABILITY

## Lead contact

Further information and requests for resources and reagents should be directed to and will be fulfilled by the lead contact, Zhiyu Zhou ([zhouzhy23@mail.sysu.edu.cn](mailto:zhouzhy23@mail.sysu.edu.cn)).

## Materials availability

This study did not generate new unique reagents.

## Data and code availability

All data reported in this article will be shared by the [lead contact](#) on request.

The single-cell RNA-seq raw data are available at the NCBI's Sequence Read Archive (SRA) data repository with the accession ID PRJNA792884.

Any additional information required to reanalyze the data reported in this article is available from the [lead contact](#) on request.

## EXPERIMENTAL MODEL AND SUBJECT DETAILS

### Animals

Mice were handled at Laboratory Animal Center of Sun Yat-sen University. All manipulations in the present study were approved by the Institutional Animal Care and Use Committee (SYSU-IACUC-2020-000428). Mice utilized in this study were all C57BL/6J genetic background (). For sc-RNA seq, mice at four postnatal stages were selected, including points marking neonatal limb development without SOC formation (P1, n = 5, mixed gender), initiation of SOC formation (P5, n = 3, mixed gender), formation of SOC prototype (P14, n = 3, male), and progression of limb maturation (P28, n = 3, male). The experimental unit was the individual mouse and mice at each time point were from one cage to guarantee unconfused developmental stage in each group.

To verify the sc-RNA seq results, mixed gender mice at postnatal 1 day (P1), 2 days (P2), 4 days (P4), 5 days (P5), and 8 days (P8), and male mice at postnatal 14 days (P14), 28 days (P28), and 2 months (M2) of age (n = 4 in each group) were utilized in the immunofluorescence study. The experimental unit was the individual mouse and mice at each time point were from different cages. Embryonic mice at different stages were also used to study the evolution of specific cell clusters during before (E14.5, n = 6) and after joint cavitation and morphogenesis (E16.5, n = 5). The experimental unit was the individual pregnant mouse.

Male mice at 10 weeks of age were chosen for establishment of osteoarthritis model. Briefly, after inhalation anesthesia with isoflurane, the anterior cruciate ligament was transected (ACLT) surgically to induce mechanical instability-associated osteoarthritis of the left knee. Sham operations were performed on other groups of mice by cutting the knee capsule and infrapatellar fat pad without performance of anterior cruciate ligament transection (ACLT). For the time-course experiments, mice were euthanized at 1, 2, 4, or 8 weeks after surgery (n = 5 in ACLT group, and n = 4 in sham group). The experimental unit was the individual mouse. The randomized digital table was used during establishment of ACLT or sham model.

## METHOD DETAILS

### Preparation of single-cell suspension

Mice were euthanized by cervical dislocation. After cleaning the hindlimbs with 75% ethanol, cut off the skin and dissociate the limbs. Carefully remove the soft tissues under the stereoscope, and segregate tibia and femur by dissecting the connective ligaments using Vannas Spring Scissors (Fine Science Tools, 150008). Tissues containing the proximal tibial growth plate to knee articular cartilage, and distal femoral growth plate to knee articular cartilage were dissected for further experiments. Samples harvested from same age of mice were pooled together and transferred to digestion medium containing with 1 mg/mL Collagenase D (Roche, 11088866001), 1mg/mL STEMxyme1 (Worthington, LS004106), and 1 mg/mL Dispase II (ThermoFisher Scientific, 17105041) in DMEM/F12 supplemented with 2% FBS for pre-treatment for 1 hour at 37°C with agitation (180 rpm) to further eliminate the soft tissues. And then, tissues were minced into pieces of about 2 mm<sup>3</sup> and digested in the freshly prepared digestion medium as above mentioned. After 20 mins of digestion, the isolated cells were collected and undissociated tissues underwent a second digestion. After 3-times repeat of digestion and collection, all dissociated cells of each group were mixed together and filtered through a 40 μm filter (Falcon, 352340) into a collection tube.<sup>137</sup> Cell counting was performed both automatically (JIMBIO, Changzhou, China) and manually (BRAND, BR717810). Triple-staining using Hoechst 33342 (Invitrogen, R37605), calcein AM (Invitrogen, C1430), and propidium iodide (PI, Invitrogen, P3566) was applied to detect cell viability.

### Construction of scRNA-seq libraries, quality control, and sequencing

Construction of scRNA-seq libraries was strictly performed according to the instructions utilizing Chromium Single Cell 3' Reagent Kits v3 (PN-1000075, PN-1000073, PN-120262). Cell suspensions containing than 85% viable cells, less than 10% doublets and no large cell aggregates were identified as qualified samples. According to cell counting results, cells were resuspended at 1,000 cells/mL to prepare the reaction mix. After loading the Chromium Single Cell Chip B (10× Genomics, 2000060), the Chromium Controller was used to generate the Gel Bead-in-Emulsion (GEMs). Immediately following that, the reverse transcription (RT) was performed to produce the barcoded, full-length cDNA from poly-adenylated mRNA released

from the captured cells. Then, the first-strand cDNA was purified and amplified to generate sufficient mass for library construction. Enzymatic fragmentation and size selection were used to optimize the cDNA amplicon size. After sequential adding of P5, P7, a sample index and TruSeq Read 2, the libraries were constructed. After quality control by Agilent 2100 Bioanalyzer, the libraries were sequenced on Illumina HiSeq X ten PE150 platform in 150 bp pair-ended manner (Novogene Technology Co., Ltd., Tianjin, China).

### Processing of scRNA-seq data

Sequencing data from 10× Genomics were processed with Cell Ranger (version 3.0.1) for demultiplexing, barcode processing, and single-cell 3' gene counting. The mm10 mouse transcriptome (UCSC) was used for sequence alignment. An internal collection of numerical multidimensional datasets by velocity from cell ranger data was extracted as loom files. Only confidently mapped, non-PCR duplicates with valid barcodes and unique molecular identifiers were used to generate the gene-barcode matrix that contained 28,386 cells.

We used Scanpy package<sup>135</sup> (version 1.7.2) for further analyzes and exploration of our single cell RNA sequencing data, such as quality filtering, dimension reduction using Principal Component Analysis (PCA) and Uniform Manifold Approximation and Projection (UMAP), unsupervised graph-based clustering, and so on. We only retained cells with more than 500 genes and less than 6,000 genes detected and less than 7% of mitochondrial genes. Then, 8,434 cells passed the filter standards. On average, we detected 3,282 genes expressed in each individual cell.

R package Monocle 2<sup>45</sup> (version 2.8) was used for pseudotime analysis. We limited the dataset to only interested cells for the analysis. We selected the high dispersion genes across cells with mean expression  $\geq 0.1$  and empirical dispersion  $\geq 0.1$  as the ordering genes for the trajectory reconstruction, using the nonlinear reconstruction algorithm DDRTree. Genes that varied across pseudotime were calculated using the Differential Gene Test function and a cutoff of adjusted *p* value  $< 0.1$  was applied. This was applied on the entire pseudotime range and also on the pseudotime intervals specific to limited cell clusters in order to avoid limitation to the genes characterized by monotonic changes across the inferred trajectory. Further branch analysis was applied using BEAM algorithms.

GO enrichment analyses<sup>58</sup> were performed using ClusterProfiler in R package<sup>136</sup> and a cutoff of adjusted *p* value  $< 0.05$  was applied, applying the Benjamini–Hochberg false discovery rate correction for multiple testing.

DEGs were identified by non-parametric Wilcoxon rank sum test and Logic regression analysis among individual clusters, and t-test was used when there were just two clusters. According to the filtered DEGs and the expression pattern, we then performed hierarchical clustering.

The Animal Transcription Factor DataBase (AnimalTFDB 3.0) was referenced to identify TFs among DEGs,<sup>138</sup> and the Cell Surface Protein Atlas was applied in recognition of surfaceome proteins.<sup>139</sup>

### Limb tissue preparation and cryosection

To time mouse pregnancy accurately, one male mouse cohabited with 2 female mice in each cage for 16 hours until the next morning in addition to checking the vaginal plugs, and then separate the female ones. The day of separation was considered as E0.5. After 11 days, 13 days, and 16 days of separation, according to changes in appearance of the pregnant female mice, including more prominent nipples and expanded waistline, the pregnant mice were euthanized and embryos were isolated and fixed with 4% paraformaldehyde (PFA, Biosharp, BL539A) overnight. After washing with 1× phosphate-buffered saline (PBS, Solarbio, P1000) for 3 times (20 min each), the hindlimbs were dissected under the stereoscope. Specimens of E16.5 was then decalcified overnight at 4°C in a solution containing 10% ethylene diamine tetra acetic acid (EDTA, Leagene, DD0002). After washing with 1× PBS buffer, specimens were incubated into cryoprotectant solution containing with 20% (w/v) sucrose (Biofroxx, 1245GR500) and 1% (w/v) polyvinyl pyrrolidone (PVP, Sigma, P5288) for 24 hours for cryoprotection. At last, Tissue-Tek® O.C.T. Compound (Sakura Finetek, 4583) was used to embed the tissue specimens for further cryosections.

The postnatal mice at different ages, and the one utilized in establishment of osteoarthritis or Sham models were euthanized. 1× PBS buffer (100 mL) and 4% PFA solution (60 mL) were used in transcardial perfusion

sequentially. Then the hindlimbs or experimental left hindlimbs were dissected and the soft tissues were removed. The specimens were transferred into 4% PFA solution for fixation followed by decalcification carried out overnight for neonates (postnatal 1–10 days), 24 h for juveniles (2–4 weeks old), and 48 hours for adults (8–18 weeks old). Cryoprotection, embedding, and cryosectioning were handled as above mentioned.

### Immunofluorescent staining

Remove the tissue sections from  $-20^{\circ}\text{C}$  and allow to thaw at room temperature (RT) for 20 min. Dry the sections at  $37^{\circ}\text{C}$  for 1 h and recover to RT for 20 min. Rehydrate the sections by incubating in  $1\times$  PBS buffer for 15 min and draw margins around the tissue section using a ImmEdge Pen (Vector, H4000). Add  $100\ \mu\text{L}$  permeabilization solution containing with 0.3% (vol/vol) Triton X-100 (Sigma, T8787) in  $1\times$  PBS buffer and incubate at RT for 30 min followed by blocking with the solution containing with 5% BSA (Biofroxx, 4240GR100) or 10% donkey serum (Solarbio, SL050) and 0.1% Triton X-100. After removing the blocking solution, add  $100\ \mu\text{L}$  primary antibody solution immediately to each section and incubate at  $4^{\circ}\text{C}$  overnight. After primary antibody incubation, wash the sections with  $1\times$  TBST buffer (Biosharp, BL315B) at RT for three times (15 min each). Add  $100\ \mu\text{L}$  secondary antibody solution and incubate at RT for 1 h. Wash with  $1\times$  TBST buffer at RT for three times (15 min each) and with  $1\times$  PBS buffer once shortly. Discard the PBS buffer from the sample and immediately add one drop of mounting medium containing with DAPI (Abcam, ab104139) avoiding air bubbles. Seal the edges with nail polish and keep the slides at  $-20^{\circ}\text{C}$  until confocal imaging (LSM880, ZEISS).

The above procedures were referred to the protocol published by Anjali P Kusumbe et al.<sup>140</sup>

### QUANTIFICATION AND STATISTICAL ANALYSIS

Limbs at each postnatal stage were pooled for scRNA-seq. The cell fraction of different cell subsets at each time point and of cells from different time point in each subset was calculated, respectively. The Differential Expressed Genes (DEGs) were determined by the non-parametric Wilcoxon rank-sum test and Logic regression analysis as part of the Scanpy package, and t-test was used when there were just two clusters. When screening cells based on marker gene expression, the threshold was set to 1.5. Both the  $p$  values and the adjusted  $p$  values were reported in the scRNA-seq data.